Degradation of a Leather-Dye by the Combination of Depolymerised Wood-Chip Biochar Adsorption and Solid-State Fermentation with Trametes Villosa SCS-10

Santiago Ortiz Monsalve (santiortizm@gmail.com)
Grupo de investigación en Micología (GIM), Facultad de Ciencias, Universidad Santiago de Cali, Cali, Colombia. VEDAS Corporación de Investigación e Innovación (VEDAS CII), Medellín, Colombia
https://orcid.org/0000-0003-4200-0466

Mariliz Gutterres
Departamento de Engenharia Química, Laboratório de Estudos em Couro e Meio Ambiente, Universidade Federal do Rio Grande do Sul, Porto Alegre, Brasil

Patrícia Valente
Departamento de Microbiologia, Imunologia e Parasitologia, Laboratório de Micologia, Universidade Federal do Rio Grande do Sul, Porto Alegre, Brasil

Jersson Plácido
Institute of Life Science (ILS 1), Swansea University Medical School, Swansea University, Swansea, Wales, UK. VEDAS Corporación de Investigación e Innovación (VEDAS CII), Medellín, Colombia

Sandra Bustamante-López
Institute of Life Science (ILS 1), Swansea University Medical School, Swansea University, Swansea, Wales, UK. VEDAS Corporación de Investigación e Innovación (VEDAS CII), Medellín, Colombia

Diane Kelly
Institute of Life Science (ILS 1), Swansea University Medical School, Swansea University, Swansea, Wales, UK

S.L. Kelly
Institute of Life Science (ILS 1), Swansea University Medical School, Swansea University, Swansea, Wales, UK

Research

Keywords: White-rot fungi, mycoremediation, solid-state fermentation, adsorption and biodegradation, biochar, biomass, leather-dyes

Posted Date: October 7th, 2020

DOI: https://doi.org/10.21203/rs.3.rs-85912/v1

Version of Record: A version of this preprint was published at Bioresources and Bioprocessing on November 25th, 2020. See the published version at https://doi.org/10.1186/s40643-020-00349-z.

Degradation of a leather-dye by the combination of depolymerised wood-chip biochar adsorption and solid-state fermentation with *Trametes villosa* SCS-10

S. Ortiz-Monsalve[1,2,3*], M. Gutterres[2], P. Valente[4], J. Plácido[1,5], S. Bustamante-López[1,5], D. Kelly[1] and S.L. Kelly[1*]

1. *Institute of Life Science (ILS 1), Swansea University Medical School, Swansea University, Swansea, Wales, UK.*

2. *Departamento de Engenharia Química, Laboratório de Estudos em Couro e Meio Ambiente, Universidade Federal do Rio Grande do Sul, Porto Alegre, Brasil.*

3. *Grupo de investigación en Micología (GIM), Facultad de Ciencias, Universidad Santiago de Cali, Cali, Colombia.*

4. *Departamento de Microbiologia, Imunologia e Parasitologia, Laboratório de Micologia, Universidade Federal do Rio Grande do Sul, Porto Alegre, Brasil.*

5. *VEDAS Corporación de Investigación e Innovación (VEDAS CII), Medellín, Colombia.*

[*] Corresponding author
Address: Institute of Life Science 1, Medical School, Swansea University, Swansea SA2 8PP, UK
Phone : +44 1792 503430
Fax : +44 1792 503430
Correspondence e-mail: santiago.ortiz@ufrgs.br; s.l.kelly@swansea.ac.uk

ABSTRACT

Adsorption into biochar-derived materials and mycoremediation are promising technologies for removing dyes from solid and liquid matrices. This study presents a combined treatment with adsorption into wood-chip biochar and mycodegradation under solid-state fermentation by *Trametes villosa* for removing the leather-dye Acid Blue 161. In the first stage, untreated wood-chip biochar, NaOH-depolymerised-biochar and $KMnO_4$-depolymerised-biochar were assessed for their dye removal efficiency by adsorption. $KMnO_4$-depolymerised-biochar exhibited the highest adsorption (85.1 ± 1.9%) after 24 h of contact. $KMnO_4$-depolymerisation modified some physical and chemical properties on the untreated wood-chip biochar, increasing the surface area (50.4 m^2 g^{-1}), pore size (1.9 nm), and presence of surface functional groups. Response Surface Methodology coupled with a Box-Behnken design was used to optimise the AB_{161} adsorption into the $KMnO_4$-depolymerised-biochar. The optimised conditions, pH 3.0, dye concentration 100 mg L^{-1} and sorbent dosage 2 g L^{-1}, led to a higher dye removal efficiency by adsorption (91.9 ± 1.0%). In a second stage, the wood-chip biochar supplemented with nutrients (1% malt extract and 0.5% peptone) was employed as a solid matrix for growing *T. villosa* and regenerating the dye-saturated material. After 15 days, *T. villosa* was able to grow (86.8 ± 0.8%), produce Laccase activity (621.9 ± 62.3 U L^{-1}), and biodegrade (91.4 ± 1.3%) the dye adsorbed into the $KMnO_4$-depolymerised-biochar. Finally, the mycoregenerated was reutilised in a new cycle of adsorption reaching 79.5 ± 2.0% of dye removal efficiency by adsorption. This study revealed the potential of the combined treatment and is an initial assessment for developing commercial alternatives for treating leather industry wastewaters.

Keywords: White-rot fungi, mycoremediation, solid-state fermentation, adsorption and biodegradation, biochar, biomass, leather-dyes.

INTRODUCTION

The worldwide production of dyes has increased to satisfy the demand of different industries such as paper and pulp, textile, and leather. Wastewaters from these industries must be treated appropriately to avoid environmental issues. Besides textile, the leather industry is one of the main industries responsible for releasing dye-containing wastewaters. Tanneries contribute to about 8% of the worldwide release of dyes in the environment (Katheresan et al. 2018). Despite this, the treatment of dye-containing wastewaters from tanneries has been less studied than that other industries. Although both textile and leather industries employ similar dyestuffs, leather-dyes have different chemical structures from textile-dyes, since they are synthesised to dye different types of materials (cotton and leather fibres). Acid dyes are the most commonly used dyestuff in the leather industry. Among them, azo and metal complex dyes are preferred due to their broad spectrum of shades, colour quality and uniformity they confer to the final product. Furthermore, wastewaters produced in textile and leather processes may have different characteristics such as pH, total organic carbon, chemical oxygen demand, and chemicals concentration, among others (Pandi et al. 2019).

Wastewaters polluted with dyes are usually related to environmental problems including inhibition of aquatic photosynthesis, depletion of dissolved oxygen and a high concentration of metals such as chromium, cobalt, and copper. In some cases, dyeing effluents can also be associated with health problems, acute and chronic toxicity, carcinogenic and mutagenic effects (Katheresan et al. 2018; Vikrant et al. 2018).

The development of advanced, cost-effective and environment-friendly technologies for treating tannery wastewaters is still necessary to preserve the natural resources. Adsorption has been a widely used technology for removing dyes and other recalcitrant compounds from wastewaters. Activated carbon is the most commonly employed adsorbent because of its

excellent adsorption capacities. However, activated carbon production is an expensive and high energy demanding process (Sumalinog et al. 2018; Dai et al. 2019). Various alternative materials have been efficiently utilised as adsorbents of synthetic dyes including leather waste (Gomes et al. 2016), cattle hair waste (Mella et al. 2017), algae and fungal biomasses (Da Fontoura et al. 2017; Puchana-Rosero et al. 2017) and biochar-derived materials (Chen et al. 2018; Zazycki et al. 2018).

Biochar has recently acquired great relevance because of its high adsorption performance and low cost (Jiang et al. 2018). Biochar is a carbonaceous by-product from biomass thermal conversion (gasification and pyrolysis), produced from a variety of low-cost and waste-derived feedstocks (Chen et al. 2018; Zazycki et al. 2018). Biochar properties include abundant surface functional groups, high surface area, porosity and stability (Braghiroli et al. 2018; Dai et al. 2019; Oliveira et al. 2017). Biochar chemical depolymerisation has been used for the production of chemicals and advanced nanomaterials such as carbon dots, humic substances and nanosilica (Placido and Capareda 2015; Placido et al. 2019a). Although the main reason for the chemical depolymerisation is the production of advanced nanomaterials, the chemical reaction creates different modifications in the depolymerised-biochar structure that improves the adsorption capacity by modifying the surface area, porosity, pH, and presence of functional groups on its surface (Braghiroli et al. 2018).

One of the major negative aspects of adsorption is handling or removing the concentrated pollutants retained in the adsorbent. During adsorption, pollutants are accumulated on the adsorbent surface, resulting in a progressive reduction of the adsorption capacity until saturation (Salvador et al. 2015). Regeneration is a desorption or degradation process that aims to reuse or recycle the sorbent material. Dye-saturated biochar materials have been regenerated by solvent desorption (Lian et al. 2016; Vyavahare et al. 2018), chemical desorption (Bharti et al. 2019; Meili et al. 2019) and thermal desorption (Zhu et al. 2019).

Most of these methods are focused on the desorption of the biochar and did not address the further degradation of the dye. Therefore, a complementary process needs to be performed after dye adsorption to avoid the transfer of the pollutant from one matrix to another and guarantee its degradation.

Mycoremediation has been proved for removing synthetic dyes from liquid and solid matrices. In a previous study, the Brazil native fungus *Trametes villosa* SCS-10 removed 96.84% of the leather dye Acid Blue 161 in submerged-state fermentation conditions (Ortiz-Monsalve et al. 2017). Most of the studies on biodegradation of dyes are performed in submerged fermentation conditions. However, in recent years, the culture of white-rot fungi on solid matrixes appeared as an alternative treatment for textile dyes (Bankole et al. 2018; Jaramillo et al. 2017). Solid-state fermentation (SSF) is a technique in which microorganisms are cultured on a solid matrix in near-absence or absence of free water. The solid matrix acts as a support for the growth and metabolism of the microorganism (Thomas et al. 2013).

Combined treatments applying adsorption and mycodegradation have been efficient for removing textile dyes: the synthetic dye Red 40 previously adsorbed into corncob waste was biodegraded by a strain of *Trametes versicolor* under SSF conditions (Jaramillo et al. 2017). Similarly, Cibacron Brilliant Red 3B-A was biodegraded by a consortium of white-rot fungi in SSF (Bankole et al. 2018). To our knowledge, biochar and depolymerised-biochar have not been used either as an adsorbent for leather dyes or as SSF matrix, and mycoremediation in SSF has not been employed as a regeneration method for saturated biochar. Therefore, coupling biochar and SSF mycoremediation is a novel method for treating dye-containing wastewaters from the leather industry.

This study aimed to evaluate the combination of depolymerised wood-chip biochar adsorption and solid-state fermentation for biodegradation of the leather-dye Acid Blue 161 and regeneration of the sorbent matrix.

The article includes the following specific aims:

-Selection of a depolymerised-biochar as an adsorbent matrix;

-Assessment of wood-chip biochar and depolymerised-biochar as suitable supports for solid-state fermentation with *Trametes villosa* SCS-10;

-Optimisation of biochar dye removal using a Box-Behnken design (BBD) and Response Surface Methodology (RSM);

-Degradation of the adsorbed dye using solid-state fermentation (SSF) with *Trametes villosa* SCS-10;

-Reutilisation of the mycoregenerated adsorbent.

MATERIALS AND METHODS

Dye and chemicals

Acid Blue 161 (AB_{161}) was supplied by Lanxess (São Leopoldo, RS, Brazil). AB_{161} is an acid/metal complex dye with an azo chromophore, used in the leather industry (Psychochemical characteristics of AB161 are included in the Supplementary material).

Chemicals: ethanol (C_2H_5OH), methanol (CH_3OH), sodium hydroxide (NaOH), sodium chloride (NaCl), acetic acid (CH_3COOH), hydrogen chloride (HCl) and potassium

permanganate ($KMnO_4$) were purchased from Fisher Scientific (USA). ABTS (2,2′-azino-bis (3-ethylbenzothiazoline-6-sulphonic acid) and activated carbon powder were obtained from Sigma-Aldrich (USA).

Media components used for microbial growth: malt extract agar, malt extract broth, and potato dextrose agar were purchased from Oxoid (UK). All chemicals were analytical grade.

Fungal strain

Trametes villosa SCS-10 is a Brazilian native strain, isolated in a previous study and selected for its high laccase activity and efficient biodegradation of leather-dyes from aqueous solution and real wastewaters (Ortiz-Monsalve et al. 2017; 2019). *T. villosa* SCS-10 was conserved on Malt Extract Agar (MEA) at 4 °C. For inoculum preparation, the strain was reactivated by cultivation on MEA for 5 days at 30 °C.

Preparation of wood-chip biochar

Wood-chip biochar (WB), NaOH-depolymerised-biochar (NWB) and $KMnO_4$-depolymerised-biochar (KWB), were assessed for their performance as dye adsorbents and as support matrices for *Trametes villosa* solid-state fermentation. WB was kindly provided by Common Visions LTD (Swansea, Wales, UK). WB was crushed using a mortar and sieved using a 1 mm mesh. (1 mm). KWB and NWB were prepared by chemical depolymerisation of the wood-chip biochar, according to Placido and Capareda (2015). The reaction mixture consisted of wood-chip biochar (10%) and $KMnO_4$ (10%) or NaOH (10%) solutions. The chemical depolymerisation reaction was performed at 120 °C for 1 h at 15 psi in an autoclave (Priorclave, London, UK). After the chemical depolymerisation, the liquid and solid phases in

the biochar solutions were separated by centrifugation (5000 rpm for 20 min, Legend RT, Sorvall).

The solid phase (depolymerised-biochar) was washed with distilled water, recovered via vacuum filtration (0.22 µm Millex syringe filters, Millipore, USA) and dried in a convection oven at 105 °C for 24 h. NWB and KWB were stored at room temperature (20–25 °C) for further experiments.

Dye removal performance

Dye removal studies were conducted with WB, NWB, KWB and commercial activated carbon (AC). 20 mg of WB, NWB, KWB or AC were transferred into 50 mL flasks containing 10 mL of 100 mg L^{-1} of AB_{161} at pH 7.0. Flasks were incubated at 150 rpm and 25 ºC using an orbital shaker (Minitron Infors orbital shaker, Switzerland). The contact time was studied for 48 h, taking samples at 0, 3, 6, 12, 18, 24 and 48 h. Dye removal efficiency by adsorption (REA, %) was determined by measuring the solution's absorbance at the dye λ_{Max} (578 nm) (UV-Vis spectrophotometer U3310, Hitachi, Japan) and employing Equation 1.

$$REA\ (\%) = \frac{(C_0 - C_e)}{C_0} x100 \qquad \text{Equation 1.}$$

Where REA represents the dye removal efficiency by adsorption (%), C_0 (mg L^{-1}) is the concentration at t = 0 and C_e is the dye concentration at different sampling times (mg L^{-1}).

The amount of dye uptake at equilibrium (q_e) was determined using Equation 2.

$$q_e\ (mg\ g^{-1}) = \frac{V(C_0 - C_e)}{M} \qquad \text{Equation 2.}$$

Where q_e represents the amount of dye uptake per gram of sorbent at equilibrium (mg g^{-1}), V is the volume of the dye-containing solution (L), and M is the sorbent mass (g).

Characterisation of wood-chip biochar

The different biochars were characterised by microscopic, morphologic and spectroscopic techniques. The biochar with the highest REA was examined before and after the dye removal assays, in order to elucidate the uptake mechanism. A surface area analyser (Nova 4200e model, Quantachrome Instruments, USA) was used to determine the specific surface area (S_{BET}) by the Brunauer, Emmett, and Teller (BET) multipoint method and the pore size distribution by the Barret, Joyner, and Halenda (BJH) method. Phase structures were determined using X-ray diffraction (XRD; Bruker D2 Phaser X-ray diffractometer, Germany). Scanning Electron Microscopy (SEM; Hitachi S4800 SEM Microscope, Japan) was employed to analyse the surface morphology. The surface functional groups were determined by Fourier Transform Infrared Spectroscopy (FT-IR; Frontier spectrometer, Perkin Elmer, USA). FT-IR analyses were carried out in the mid-IR region of 4000−400 cm^{-1}. The point of zero charges (pH_{pzc}) of the biochars was determined using a Zetasizer NANO-Z S90 (Malvern Instruments, UK). For the pH_{pzc} analysis, the particles were suspended in ultrapure water and sonicated for 10 min. The pH was adjusted using 0.1 N HCl or 0.1 N NaOH solutions.

Optimisation of AB_{161} dye removal

A Response Surface Methodology (RSM) coupled with a Box-Behnken design (BBD) was used to determine statistically the optimum conditions for dye removal. The optimisation experiments were performed with the depolymerised-biochar with the highest REA as described above. The independent variables, pH (X_1), initial dye concentration (mg L^{-1}) (X_2) and sorbent dosage (g L^{-1}) (X_3), were studied at three different levels (–1, 0 and 1) and the response variable was REA (%).

The range and levels (coded and uncoded) of variables are listed in Table 1. Specific dye concentrations were prepared via dilutions of a stock solution containing 1000 mg L^{-1} of AB_{161} in ultrapure water. The initial pH was adjusted with 0.1 N HCl or 0.1 N NaOH solutions. The experimental design had 17 experiments, including 12 factorial points and 5 replicates at the central point (Table 2). The experimental matrix was designed using the Design Expert® v.11.0 software (Stat-ease, USA). The predicted response, dye removal (Y), was calculated with a second-order polynomial regression model (Equation 3), as follows:

$$Y = b_0 + \sum_{i=1}^{k} b_i x_i + \sum_{i=1}^{k} b_{ii} {x_i}^2 + \sum_{i=1}^{k-1} \sum_{j=2}^{k} b_{ij} x_i x_j + \varepsilon \qquad \text{Equation 3.}$$

Where Y is the predicted response value, b_0 is a constant term, b_i is the linear effect term, b_{ii} is the squared effect term, b_{ij} is an interactive effect term, x_i and x_j are independent variables, and ε is the error of the model. An experiment under the optimal dye removal conditions was performed to confirm the model's prediction.

Desorption assays

The dye-containing depolymerised-biochar (KWB-AB_{161}) obtained from the optimal condition experiments was used in the desorption assays. The KWB-AB_{161} was washed with distilled water and dried (105 °C for 24h). Hydrogen chloride, glacial acetic acid, sodium

chloride, sodium hydroxide, ethanol, methanol, and distilled water were assessed as eluents (Vyavahare et al. 2018; Daneshvar et al. 2017). Desorption experiments were conducted by mixing 20 mg of dried KWB-AB_{161} in 10 mL of each eluent solution (1 M). The mixtures were stirred at 130 rpm, 20 ºC for 120 min and then separated by centrifugation (3000 rpm for 5 min, Legend RT, Sorvall) (Daneshvar et al. 2017). Dye desorption was calculated by measuring the absorbance of the solution at the λ_{Max} of the dye (578 nm) and using Equation 4.

$$DE\ (\%) = \frac{V_e\, C_e}{M_s\, q_e} x\ 100 \qquad \text{Equation 4}$$

Where DE is the dye desorption efficiency (%), V_e is the volume of the eluent used (L), M_s is the mass of the saturated sorbent (g), C_e is final dye concentration (mg L^{-1}) and q_e is the amount of dye uptake per gram of sorbent at equilibrium (mg g^{-1}).

Solid-state fermentation in wood-chip biochar

T. villosa SCS-10 solid-state fermentation in wood-chip biochar (WB) was assessed in a single factor experiment. Four different nutrient conditions combining malt extract, glucose and peptone were evaluated (Table 3). The first condition (T_1, high nutrient supply) utilised the optimal medium composition obtained in a previous study with *T. villosa* SCS-10 (Ortiz-Monsalve et al. 2017), and consisted of 1% (w/v) malt extract, 1% (w/v) glucose and 0.5% (w/v) peptone. Additional conditions were variations of T_1 concentrations: reduced nutrient supply (T_2), low nutrient supply (T_3) (Ortiz-Monsalve et al. 2019) and without additional nutrients (T_4). The SSF process was performed in 100 mm Petri dishes containing 2 g of WB mixed with 5 mL of sterile water and nutrients. The WB Petri-dishes were inoculated with four agar plugs (diameter, 1 cm) from actively growing *T. villosa* SCS-10 and was incubated

at 30 °C for 9 days. The experiment was performed in triplicates using destructive assays for each sampling day. Fungal growth (G, %) and enzyme activity (U L^{-1}) were measured at days 0, 3, 6, 9, 12 and 15.

Fungal growth was determined with the image processing software Image J ® v. 1.48 (NIH, USA) by analysing photographic records, according to Copete-Pertuz et al. (2019). The fungal growth was expressed in terms of Growth Area (A, %) following Equation 5.

$$G\ (\%) = \frac{A}{Petri\ dish\ total\ area} x100 \qquad \text{Equation 5.}$$

Where G is the fungal growth (%), A was the growth area obtained by the Image J software at different days sampled (cm^2) and $Petri\ dish\ total\ area$ (56.7 cm^2).

Enzyme extraction and activity assays

The extracellular enzymes were extracted by transferring the content of each SSF plate into 50 mL centrifuge tubes with 20 mL of citrate-phosphate buffer (0.15 M, pH 5.0) and stirred on an orbital shaker at 4 ºC for 120 min (Jaramillo et al. 2017). After extraction, extractant and biochar were centrifuged, and the supernatant was used for ligninolytic activity measurements. Laccase (Lac) activity was determined by following the oxidation of ABTS (2 mM). The change in absorbance was monitored at 405 nm (ε_{405}=3.6×10^4 M^{-1} cm^{-1}) for 5 min. One unit of Lac activity was defined as the amount of laccase that catalysed 1 µmol of ABTS per minute (Wang and Ng 2006). Manganese peroxidase (MnP) activity was measured following the catalysis of DMP (1 mM) at pH 4.5. The increase in absorbance was determined at 469 nm (ε_{469}=2.75×10^4 M^{-1} cm^{-1}) (Martinez et al. 1996). Lignin peroxidase (LiP) was determined by monitoring the oxidation of veratryl alcohol (10 mM) at pH 3.0. The change in absorbance was measured at 310 nm (ε_{310}=9.3×10^4 M^{-1} cm^{-1}) for 3 min (Arora and

Gill 2001). MnP and LiP assays were performed in the absence/presence of cofactors (H_2O_2 and $MnSO_4$). Lac, LiP and MnP activities were expressed as U L^{-1}.

Biodegradation and regeneration of the dye-containing depolymerised-biochar by solid-state fermentation with *T. villosa*

To produce a significant amount of KWB-AB_{161}, the adsorption process was scaled up 100 times, while maintaining the optimised operational conditions determined by the RSM (pH 3.0, dye concentration 100 mg L^{-1} and sorbent dosage 2 g L^{-1}). The KWB-AB_{161} was prepared in 2-L flasks filled with 1000 mL of dye-containing solution at 100 mg L^{-1} and 2 g L^{-1} of KWB. Flasks were stirred in a shaker at 150 rpm and 25 ºC for 24 h. REA and q_e were calculated according to Equation 1 and Equation 2. At the end of the process, KWB-AB_{161} was separated by centrifugation (5000 rpm for 10 min), washed with distilled water and dried in an oven (105 °C for 24 h).

The solid-state fermentation (SSF) was performed in Petri dishes. 2 g of dried KWB-AB_{161} were mixed with 5 mL of water and supplemented with the T_2 nutrient condition (1% malt extract, 0.5% glucose and 0.5% peptone). KWB-AB_{161} was inoculated with 4 agar plugs (diameter, 1 cm) from actively growing *T. villosa* SCS-10 and incubated at 30 °C for 15 days. Lac, MnP and growth were measured as previously described (Section 2.9) and reported at days 0, 3, 6, 9, 12 and 15. In order to find the dye biodegradation achieved by *T. villosa* SCS-10 during the SSF, the plates' content was subjected to a desorption process with ethanol (1 M) following the protocol described in Section 2.7. A comparison between the desorption

efficiency before and after the SSF was used to determine the dye removal efficiency by mycoremediation (REM,%), according to Equation 6.

$$REM\ (\%) = \frac{(m_a - m_d)}{ma} x100 \qquad \text{Equation 6.}$$

Where REM represents the dye removal efficiency by mycoremediation (%), m_a is the mass of desorbed dye from KWB-AB_{161} before the SSF and m_d is the mass of desorbed dye from KWB-AB_{161} after the SSF sampled at different days.

Reutilisation assays of the mycorgenerated biochar

The biochar recovered from the SSF was considered as mycoregenerated-KWB (MKWB), and it was tested in a new adsorption cycle. MKWB was obtained after 15 days of SSF with *T. villosa*, harvested and dried in a convection oven at 50 °C for 24 h (Zeng et al. 2015). The weight difference between mycelia and MKWB facilitated their separation during drying, and the remaining mycelia were manually removed with a clamp. The dye removal assays were carried out at the optimised conditions described above (pH 3.0, initial dye concentration 100 mg L^{-1} and sorbent dosage 2 g L^{-1}). 20 mg of MKWB were transferred into 50 mL flasks containing 10 mL of AB_{161} solution (100 mg L^{-1}) at pH 3. Flasks were incubated at 150 rpm and 25 ºC for 24 h. REA and q_e were determined using Equation 1 and Equation 2, respectively.

RESULTS AND DISCUSSION

Dye removal performance

An initial screening of the dye removal performance of wood-chip biochar derived materials (WB, NWB, and KWB) was carried out using the leather-dye Acid Blue 161 (AB_{161}). The results obtained were compared with commercial activated carbon (AC). The contact time (0 to 48 h) was analysed to determinate the equilibrium time for maximum removal. The dye removal efficiencies by adsorption (REAs) are shown in Figure 1. It can be observed that all the biochars removed AB_{161} to a different extent. After 48 h, the highest REA was displayed by AC (93.5 ± 0.9%) followed by KWB (85.7± 1.7%). The depolymerised-biochar exhibited a higher REA than its precursor WB (46.1 ± 1.7%).

In the case of KWB and AC, the AB_{161} removal increased sharply within the first 3–24 h and after 24 h remained relatively constant with time, reaching the equilibrium. Hence, 24 h was selected as KWB contact time. NWB and WB's REAs increased during the first 6 h of treatment; however, they did not change significantly after 12 h. WB and NWB's REAs were significantly lower than that of KWB (the ANOVA and Duncan's test are presented in the supplementary material). The highest amounts of dye uptake (q_e) were also obtained with AC (47.9 ± 1.5 mg g^{-1}) and KWB (43.9 ± 0.4 mg g^{-1}). The high REA and q_e values displayed by commercial activated carbon were related to its well-known characteristics as adsorbent (great surface area, high ion exchange capacity and strong affinity to organic and inorganic compounds) (Nautiyal et al. 2016; Sewu et al. 2017; Sumalinog et al. 2018). Though, it should be noted that KWB's REA was 8% less than that obtained with AC. The high REA of KWB indicates its potential for removing AB_{161} from wastewaters. Different from activated carbon, WB and KWB are by-products from waste-to-energy processes and advanced material production where chemicals and carbonaceous nanomaterials are synthesised (Das et al. 2018; Oliveira et al. 2017; Placido et al. 2019a). The use of wastes makes biochar from these processes a superior economic and environmentally friendly option than activated carbons.

Characterisation of wood-chip biochar derived sorbents

Some physical and chemical properties of WB and KWB were analysed to elucidate the dye removal phenomena. KWB was characterised before and after AB_{161} removal assays because it displayed the highest REA and q_e in the dye removal screening. Table 4 shows some physicochemical properties of WB and KWB.

XRD diffraction analyses evidenced that WB and KWB did not exhibit sharp peaks, indicating the non-crystalline nature of the materials and suggesting amorphous structures (Figure 2a). The empty spaces in the disordered structures of both WB and KWB allowed the coupling of AB_{161} molecules with their surface functional groups. A similar crystalline nature was described by XRD diffraction analyses of pecan nutshells biochar (Zazycki et al. 2018), microalgae biochar (Behl et al. 2019) and saccharide-derived biochar (Tran et al. 2017).

The BET surface areas (S_{BET}) were 3.40 $m^2\ g^{-1}$ (WB) and 50.4 $m^2\ g^{-1}$ (KWB). KWB evidenced a significant augment in the S_{BET} (approximately 15-fold). The average pore size of KWB (1.9 nm) was also higher than that of WB (0.6 nm). WB and KWB were classified into the microporous region (average pore size < 2.0 nm) (Thommes et al. 2015). According to the International Union of Pure and Applied Chemistry (IUPAC), the KWB N_2 adsorption/desorption isotherm was classified as Type 4 with an H_4 hysteresis loop (Figure 2b), a typical characteristic of micro-mesoporous carbon materials (Thommes et al. 2015). $KMnO_4$ is a strong oxidising agent that might deform some nanoporous and microporous structures on the biochar surface, creating new MnO-structures which led to the formation of more and larger micro-mesopores (Song et al. 2014). The $KMnO_4$ reaction increased KWB's surface area, offering more and larger active sites for interacting with AB_{161} molecules. The

depolymerisation also enhanced KWB's pore size, facilitating the pore diffusion of dye molecules. These results suggested that physisorption (physical adsorption) via pore diffusion was involved in the dye removal mechanism by KWB. Previously, Jiang et al. (2018) augmented the specific surface area and total pore volume of swine manure biochar with a $KMnO_4$ reaction of the raw material. The chemical modification on the biochar surface improved the adsorption capacity of metals (Cu^{2+} and Zn^{2+}) and antibiotics. Similarly, Song et al. (2014) augmented the surface area and porosity of corn straw biochar by $KMnO_4$ reaction, improving the Cu (II) adsorption capacity of corn straw biochar.

FT-IR spectroscopy was utilised to determine the changes in the surface functional groups during the treatment. FT-IR spectra of WB and KWB, before and after AB_{161} removal, are shown in Figure 2c. All the wood-chip biochar derived sorbents displayed similar FT-IR profiles, related to common polymers from woody biomass. The bands between 3500–3300 cm^{-1} indicated the –OH stretching of phenol and alcohol groups associated with cellulosic-derived materials (Chaukura et al. 2017; Zazycki et al. 2018).

The non-depolymerised WB had several functional groups on the surface, with signals at 3350 cm^{-1} (–OH stretching), 1700 cm^{-1} (COOH, C=O stretching), and 750 cm^{-1} (aromatic C–H) (Boakye et al. 2019). The peaks at 1590 and 1390 cm^{-1} were related to C=C–C stretch and C=C skeletal vibrations (Sewu et al. 2017; Bernardino et al. 2017). The peak at 1200 cm^{-1} was related to C–O–H symmetric bending vibrations (Xu et al. 2016).The FT-IR spectrum of the KWB showed signals at 1580, 1390 and 750 cm^{-1}related to carbon linkages and the disappearance of peaks at 1200 and 1700 cm^{-1}, also related to carbon vibration, indicating that the depolymerisation process generated chemical modifications to the biochar structure, where carbonaceous compounds were released into the liquid phase producing a reduction of carbonaceous linkages signals (Placido et al. 2019a; 2019b). Additionally, it should be noted that bands at 3350, 1350 and 1250 cm^{-1}, ascribed to O-containing groups, exhibited enhanced

intensity. The $KMnO_4$ depolymerisation augmented the number of Mn–O bonds, modifying O-containing functional groups, especially the C–O bond (1350 cm^{-1}) and OH stretching (3350 cm^{-1}) (Jiang et al. 2018; Song et al. 2014). New intense peaks in the FTIR profile of KWB were detected between 400–500 cm^{-1} and were associated with the presence of K–OH (Placido et al. 2019c). Carboxyl groups act as electron acceptors leading to the formation of π–π-electron-donor-acceptor interaction with aromatic molecules on the dye structure. Hydroxyl groups in biochar surface act as π-electron-donor sites (Dai et al. 2019).

After dye removal, the KWB-AB_{161} FTIR spectra exhibited the change and disappearance of many peaks demonstrating the interactions between KWB surface functional groups and the AB_{161} molecules. The phenolic functional group's peak shifted (from 3350 to 3333 cm^{-1}) and reduced its intensity, exposing its participation in the removal phenomena. Similarly, the disappearance of the signals at 1350 and 1250 cm^{-1} confirmed the involvement of carboxyl functional groups on the dye removal process. These data were in accordance with previous studies with biochar (Xu et al. 2016; Sewu et al. 2017; Ahmed et al. 2019). The appearance of new signals at 950 and 595 cm^{-1} can be related to S=O and C–N stretching vibrations, evidencing the presence of AB_{161} on the biochar as those chemicals bonds belonging to the AB_{161} structure (Supplementary material). The FT-IR results offered more evidence about the dye removal mechanism. The $KMnO_4$ depolymerisation provided a stronger presence of functional groups in the surface, mainly active oxygen-containing groups such as hydroxyl (–OH) and carboxylic (–COOH). FT-IR results revealed the possible participation of physisorption mechanisms via electrostatic attraction/repulsion interactions between the functional groups on the KWB surface and the AB_{161} molecules, as additional mechanisms to pore diffusion.

Zeta potential measurements determined the pH value corresponding to the point of zero charges (pH_{pzc}). KWB zeta potential decreased from about 10.0 mV at pH 3.0 to 1.0 mV

at pH 4.5. The pH_{pzc} of KWB was obtained at pH 4.6. Then, the Zeta potential decreased gradually to about -30 mV at pH>7.0 (Figure 2d). The pH_{pzc} of WB was 5.1, similar to other lignocellulosic-derived biochar as switchgrass biochar (pH_{pzc}=5.1) (Park et al. 2019), sugarcane bagasse biochar (pH_{pzc}=5.3) (Vyavahare et al. 2018) and wood-chip biochar (pH_{pzc}=6.0) (Wathukarage et al. 2017). According to data, the pH_{pzc} of WB reduced with the KMnO4 depolymerisation. For pH values lower than 4.6, KWB had a positive surface charge. When the pH value of the solution was higher than pH_{pzc}, the KWB was negatively charged. Biochar-derived materials have numerous functional groups, whose ionisation potential strongly depends on their pH. Thus, the biochar surface charge is also pH-dependent. The charge on the biochar surface can affect the electrostatic attraction between biochar and organic dyes. For pH values<pH_{pzc}, attraction occurs between the positively charged biochar surface and negatively charged compounds. In contrast, when pH>pH_{pzc}, the negatively charged biochar surface attracts cationic compounds (Jiang et al. 2018). The initial dye removal assays were carried out at neutral pH (pH=7.0 > pH_{pzc}). At pH 7.0, the KWB surface was negatively charged. AB_{161} is an anionic dye with sodium sulfonate groups, negatively charged in aqueous solutions (Aksu et al. 2008; da Fontoura et al. 2017). These initial results suggested that electrostatic attraction was a weaker mechanism than pore diffusion. However, these phenomena were further studied in the optimisation and desorption experiments.

SEM micrographs (Figure 3) agreed with the BET/BEJ and XRD results. WB had a homogenous structure to a certain extent, with visible pores on its surface. In contrast, KWB displayed a more heterogeneous structure with a rougher surface, higher superficial area, and multiple protuberances, cavities and pores. SEM micrographs confirmed the structural changes by the depolymerisation reaction. The thermochemical activation carried out on KWB, led to the formation of grooves, pores and cavities with different sizes on the material,

which is adequate for dye removal. These cavities and porous were larger in KWB than WB, allowing a higher penetration of AB_{161} molecules. Although KWB surface was rough after the dye removal assays, it displayed a smooth packing of pores and cavities related to dye presence (Chaukura et al. 2017; Zazycki et al. 2018).

The characterisation analyses evidenced that the $KMnO_4$ reaction provided a greater surface area, larger pore size, and a higher presence of functional groups in the wood-chip biochar surface. These proprieties are related to high adsorption capacity. Therefore, the depolymerisation with $KMnO_4$ improved the adsorptive capacity of the biochar.

Dye removal by KWB was an adsorption process, where the AB_{161} molecules were transferred from the aqueous solution to the biochar surface attracted by physical forces and bonds with KWB functional groups. Physisorption via pore diffusion, π–π electron-donor acceptor interactions and OH-bonding were postulated as the mechanisms involved in AB_{161} removal. Since the aim of this study was to evaluate the treatment of AB_{161} by the combination of wood-chip biochar adsorption and mycodegradation in solid-state fermentation with *T. villosa*, kinetic and thermodynamic studies were not addressed.

Optimisation of AB_{161} dye sorption into KWB

A Box-Behnken design (BBD) was applied to establish the combined effect of the three selected independent variables, pH (X_1), initial concentration of dye (X_2) and sorbent dosage (X_3), on the dye removal efficiency by adsorption (REA) and to determine the optimal conditions for the dye adsorption. As seen in Table 2, the predicted and experimental values of REA were very similar. The dye removal efficiency quadratic prediction model is described in Equation 7.

$$Y = 80.7 - 4.03\,X_1 - 19.45\,X_2 + 2.2\,X_3 + 3.68\,X_1X_2 + 1.78\,X_1X_3 + 0.675\,X_2X_3 - 3.24\,X_1^2 - 12.39\,X_2^2 - 3.74\,X_3^2 \quad \text{Equation 7.}$$

Where Y represents the dye removal efficiency by adsorption (REA, %), X_1 is the pH, X_2 is the initial dye concentration (mg L^{-1}) and X_3 is the sorbent dosage (g L^{-1}). The quadratic prediction model was statically significant to represent the response, and the lack of fit was not significant (Lack of fit = 0.0602>0.05). The predicted R^2 of 0.984 was in reasonable agreement with the adjusted R^2 of 0.990, confirming the prediction accuracy of the developed model. The model's ANOVAs are included in the supplementary material.

Figure 4a displays the model accuracy by comparing the predicted and experimental dye removal for each run. Figure 4b–d illustrates the response surface plots of the mutual effect of two variables on REA, while the third variable was kept constant at level 0. The double effect of the initial dye concentration and pH is shown in the three-dimensional response surface (Fig. 4b). Both of the variables had a significant effect on REA. The initial dye concentration played an important role in dye removal as REA decreased with the increase in dye concentration from 100 mg L^{-1} to 300 mg L^{-1}. These results suggested the saturation of the active sites and reduction of the available surface area of the adsorbent, which agrees with the KWB SEM images.

Similarly, the pH also had a strong influence on REA as dye molecules have different ionisation potentials with the pH; thus, the dye net charge is also pH-dependent (Mella et al. 2017). KWB had a pH_{pzc} of 4.6, and at pHs below this value, KWB had a positive surface charge. Then, at lower pH, electrostatic attraction took place between the positive surface charge of KWB and the negative charge of AB_{161}. In contrast, when the pH increased, the repulsion between OH^- ions and the negatively charged groups in the dye arose, affecting the REA. These results were consistent with previous reports about using acidic conditions (pH

2.0–4.0) as optimal for the adsorption of AB_{161} into dried fungal and microalgae biomasses (da Fontoura et al. 2017; Puchana-Rosero et al. 2017). These conditions are significant for treating real effluents because leather dyeing wastewaters are generally acid, ranging between 3.0–4.0 (Mella et al. 2017). Figure 4c depicts the mutual effect of the initial dye concentration and adsorbent dosage. REA increased at higher adsorbent dose, since the number of active sites/pores available on KWB for binding the AB_{161} molecules augmented. These results were in accordance with previous studies, where greater adsorption of AB_{161} was obtained with a higher dosage of adsorbents (da Fontoura et al. 2017; Mella et al. 2017).

The optimised parameters for maximising the REA were pH 3.0, initial dye concentration 100 mg L^{-1} and sorbent dosage 2 g L^{-1}. Under these conditions, the predicted REA was 93%. In order to validate the RSM based on the BBD model, quintuplicate experiments were performed in the selected optimal conditions. In the optimal conditions, KWB led to a higher REA (91.9 ± 1.0%) and q_e (46.7 ± 0.4 mg g^{-1}). These results confirmed the model's validity (*p-value*<0.0001) by the similarity between the predicted (93%) and experimental (92%) REA. The optimised operational conditions obtained REA and q_e values similar to those obtained with activated carbon. A comparison between KWB and other adsorbents is also included in Table 4. KWB exhibited higher surface area and higher dye adsorption capacity than other biochar-derived materials (e.g. algae biochar or pulp and paper sludge biochar) toward different dyes (e.g. Congo Red, Methyl Orange and Methylene Blue) (Table 4).

Desorption assays

In the current study, desorption was used to remove the AB_{161} dye retained on the KWB-AB_{161} biochar and to analyse its biodegradation with *T. villosa* SCS-10. The AB_{161} desorption from KWB-AB_{161} biochar was evaluated with different eluents (Table 5). Ethanol

exhibited the maximum desorption (50.2 ± 4.76%), followed by methanol (38.6 ± 4.05%). Most solvents are polar compounds that penetrate the porous adsorbent structures, reaching active sites and physically displacing the adsorbate molecules (Salvador et al. 2015). Ethanol was the most suitable solvent as it penetrated the mesopores of KWB, affecting the polarity of functional groups such as hydroxyl and carboxylic, and displacing the AB_{161} molecules. Distilled water desorbed only 2.0 ± 0.39%, indicating the strong interaction between the AB_{161} molecules and the surface groups on KWB. NaCl and NaOH solutions exhibited lower desorption efficiency (21.2 ± 2.54 and 18.8 ± 0.92%, respectively). Acid compounds such as HCl and CH_3COOH desorbed less than 5%.

These results were consistent with the previous pH analysis and indicated that electrostatic attractions were also present in the adsorption process. All the further desorption assays were performed using ethanol (1 M).

T. villosa solid-state fermentation in wood-chip biochar

Although there are many alternatives for using biochar, to our knowledge biochar have not been used as a solid-state fermentation (SSF) matrix. In the current study, WB with four different nutrient conditions (Table 3) was used as a solid matrix for SSF with *T. villosa* SCS-10. The higher concentration of nutrients, treatment T_1, led to the highest growth (90.13 ± 0.40%). However, the reduced nutrient addition (T_2) also permitted substantial growth (86.76 ± 0.76%). The treatments with low nutrients concentration (T_3) and without nutrient supplementation (T_4) displayed a growth area ranging between 20–50%. The growth was significantly higher in the nutrient added conditions (T_1, T_2 and T_3). However, *T. villosa* slightly grew in the non-nutrient condition indicating that WB provided some nutrients for

fungal growth. Similar to growth percentage, high Lac activities (>600 UL^{-1}) were achieved on T_1 and T_2 treatments (Figure 5a). T_2 displayed the highest Lac activity (758.85 ± 51.70 U L^{-1}). In fact, this Lac activity was higher than that expressed in liquid state fermentations with the same strain (approx. 500 U L^{-1}) (Ortiz-Monsalve et al. 2017, 2019). Figure 5b illustrates the profile of fungal growth and Lac activity. The first sign of mycelium production was detected on the 3rd day of culture. The highest Lac values were reached between the 8th and 10th day of cultivation. Manganese or lignin peroxidases activities were not detected in the tested conditions. In SSF cultures, white-rot fungi grow on similar conditions as their natural habitats allowing the production of enzymes and metabolites secreted at those specific conditions (Daâssi et al. 2016).

The solid matrix could be a source of nutrients, or it could be an inert support for fungal growth (Thomas et al. 2013). The nutrient release capacity of biochar depends on feedstock nature. Wood-chip derived biochars prepared from plant-based feedstocks are potential sources of nutrient such as C, N, P, K, S Mg, Na and Cu (Singh et al. 2010; El-Naggar et al. 2019). The Lac activity and growth of *T. villosa* were strongly dependent on the C/N ratio and carbon and nitrogen sources (malt extract, glucose or peptone). Similar to SSF culture, *T. villosa* SCS-10 liquid cultures evidenced a decline in the Lac activity with higher glucose concentration. (Ortiz-Monsalve et al. 2019).

To our knowledge, studies using biochar as supports for SSF were not available in the current literature; therefore, a Lac activity comparison was made with studies employing natural-derived compounds as supports for growing *Trametes* strains (Table 6). Lac activity expressed by *Trametes villosa* SSF in WB (approx. 700 U L^{-1}) was higher than that of *Trametes* sp. in SSF of cassava residue (150 U L^{-1}) (Li et al. 2014) and *Trametes hirsuta* in SSF of pine wood-chip and orange peel (480 U L^{-1}) (Böhmer et al. 2011) and lower than that of *Trametes pubescens* in SSF of sunflower seed shells (5603 U L^{-1}) (Rodríguez-Couto et al.

2009) and *Trametes versicolor* in SSF of corncobs (911 U mL^{-1}) (Asgher et al. 2017). However, in these studies, laccase inducers, such as copper sulphate or phenols, were applied, or concentrated laccase extracts were produced. The wood-chip biochar supplemented with nutrients was considered a suitable support for the growth of *T. villosa* and Lac activity production. These results open the door to utilise biochar from thermal conversion as SSF matrices. T_2 was selected as the culture nutrient condition for the subsequent analyses because T_2 provided the best metabolic conditions for maximum Lac activity production.

Biodegradation of adsorbed AB_{161} in depolymerised biochar by solid-state fermentation with *T. villosa*

In order to produce a high amount of dye-containing biochar, the adsorption process of AB_{161} into KWB was scale-up 100-times while maintaining the optimal operational conditions. As WB was confirmed as a suitable support for *T. villosa* growth, the dye-containing depolymerised biochar (KWB-AB_{161}) was used as a matrix for the solid-state fermentation with *T. villosa* SCS-10 using the conditions selected in Section 3.5. Desorption using ethanol (1 M) was assessed before and after the SSF and data were compared to determinate the dye biodegradation efficiency of the fungal strain. KWB conserved the adsorption capacity in scale-up conditions achieving 90.1 ± 1.0% of REA. Desorption (57.8 ± 3.5%) also remained similar to the one obtained in the desorption screening (50.2 ± 4.76%). The SSF supported a fungal growth of 67.8 ± 5.6%. The growth of *T. villosa* on KWB was significantly reduced when compared to that achieved on WB (87.0 ± 2.0%). This negative effect was probably related to the toxic effect of AB_{161} on biomass production (Ortiz-Monsalve et al. 2017) or the modifications on the surface of KWB. Although the fungal growth was significantly reduced, the Lac activity peak of 751.5 ± 55.9 U L^{-1} at the 9th

day of culture was slightly higher than that of the SSF on WB (621.8 ± 62.3 UL^{-1}). A plausible explanation could be the Lac activity induction by the presence of phenolic groups in the KWB-AB_{161} surface. Chemical compounds with phenolic nature such as dyes are laccase inducers because of their similarity with lignin's molecular structure (Mann et al. 2015; Rivera-Hoyos et al. 2013).

In the current study, the initial dye concentration before adsorption was 103.4 mg L^{-1}. After KWB adsorption, approximately 10.2 mg of dye remained in the effluent, and 90.1 mg were adsorbed into the depolymerised biochar. The desorption with ethanol recovered 54.6 ± 2.0 mg of AB_{161}. This amount (54.6 mg) was selected as the initial dye mass to be removed in the solid-state fermentation.

The desorption after the SSF led to the recovery of 4.9 ± 0.4 mg of dye, indicating that *T. villosa* SCS-10 removed $91.36 \pm 1.32\%$ AB_{161} from KWB. As shown in the dye removal profile (Figure 6), decolourisation was strongly associated with Lac activity. In the first 3–6 days of solid culture, *T. villosa* removed just 10–20% of AB_{161}. However, after the 6^{th} day, the dye removal efficiency by mycoremediation (REM) increased progressively until the 9^{th} day when it reached 85%. In this period, Lac activity increased from 1001–300 U L^{-1} to 751.4 U L^{-1}, which was the highest peak of Lac activity.

Different mechanisms may be involved in dye removal by fungal treatment: breakdown of the dye structure by enzymes (biodegradation) or binding of the dye molecules to the mycelia surface (biosorption) (Kaushik and Malik 2009). *Trametes villosa* maintained its original colour after the solid-state fermentation (Figure 6b), suggesting that the main mechanism of dye removal was biodegradation (Kalpana et al. 2012; Saroj et al. 2014). In addition, during the SSF cultivation, the plate's content (KWB and mycelium) were not separated before desorption, and the biomass was also suspended in ethanol. According to

this, AB_{161} molecules that would be biosorbed in biomass were also removed in the solvent desorption. These results suggested enzymatic biodegradation as the main mechanism of dye removal in the *T. villosa* SSF.

UV-vis spectroscopy was used to complement the identification of the mechanisms involved in dye removal. UV-vis spectrum analyses (400–800 nm) of the adsorption and solid-state fermentation processes are shown in Figure 7. During the adsorption on KWB, the characteristic peak of AB_{161} at 578 nm decreased proportionally with the rest of the spectra until reaching its lowest value after 24h (Fig. 7a). In contrast, a complete decline in the characteristic peak was observed during the solid-state fermentation with *T. villosa*. Additionally, the absorbance peaks ratios of KWB-AB_{161} before and after the SSF were different (Fig. 7b), a typical behaviour related to enzymatic biodegradation of dyes (Chen and Ting. 2015).

During adsorption and biosorption processes, dye's characteristic peaks of maximum absorbance (λ_{max}) decrease proportionally in a similar ratio. Whereas, in enzyme-mediated processes, the peak reduces in different ratios, until it completely disappears or forms new peaks (Chen and Ting 2015; Kalpana et al. 2012). Therefore, laccase biodegradation was postulated as the main mechanism involved in AB_{161} removal during *T. villosa* SSF.

The REM of *T. villosa* SSF on KWB (over 90%) was similar to other studies with *Trametes* species (90–100%) using agroindustrial matrices as support for dye biodegradation. These studies reported dye biodegradation via *in vitro* and *in vivo* processes (Asgher et al. 2017; Li et al. 2014; Jaramillo et al. 2017). A comparison with these reports is presented in Table 6. Although *in vitro* biodegradation has been more efficient for treating synthetic dyes, this process may require the extraction of crude extracts, the addition of enzymatic mediators or/and inducers and may be restricted to optimal operating conditions such as specific pH or

temperature ranges. The *in vivo* degradation with *T. villosa* was efficient without the addition of inducers or mediators, or the purification of crude extracts.

Reutilisation of the mycoregenerated KWB

The mycoregenerated-KWB (MKWB, KWB after adsorption and SSF assays) was used for a new batch of adsorption, aiming a cyclic treatment. The adsorption assays utilised the optimised parameters for dye adsorption into KWB (pH 3.0, initial dye concentration 100 mg L^{-1} and sorbent dosage 2 g L^{-1}). After 24 h of adsorption, MKWB removed 79.5 ± 2.0% of AB_{161} from the aqueous solution. The decline in the REA was attributed to the saturation of surface functional groups (such as –COO and –OH). However, the q_e of MKWB (41.4 ± 1.8 mg g^{-1}) was similar to that obtained with KWB during the first batch of adsorption (46.6 ± 0.4 mg g^{-1}). In previous studies, Zeng et al. (2015) also described the regeneration of Methylene Blue dye-saturated rice residues by SSF with *Phanerochaete chrysosporium*. The SSF system led to 85% of colour removal, related with MnP activity. The mycoregenerated sorbents were used in an additional cycle of adsorption and degradation, reaching a colour removal between 65–90%. There are few studies on the regeneration of biochar after adsorption of pollutants and the further handling or degradation of the compound. This article is the first report about mycoregeneration of dye-saturated biochar. SSF with *Trametes villosa* on KWB-AB_{161} was an appropriate method for the regeneration and reuse of the saturated adsorbent. The mycodegradation of the adsorbed dye was also a simple and eco-friendly alternative for the final disposal of adsorbed AB_{161}.

CONCLUSIONS

The combination adsorption into depolymerised wood-chip biochar and solid-state fermentation (SSF) with *T. villosa* SCS-10 was an efficient and environment-friendly method for removing the leather-dye Acid Blue 161 (AB_{161}). The $KMnO_4$ depolymerised biochar (KWB) exhibited higher dye removal efficiency by adsorption (REA, 85%) by a physisorption process mediated by pore diffusion, π–π electron-donor acceptor interactions and OH-bonding. Response Surface Methodology (RSM) coupled with a Box-Behnken design (BBD) established the optimum adsorption conditions and led to a higher REA (over 90%). After the dye removal from the aqueous solution, SSF with *T. villosa* SCS-10 biodegraded 91.4% of the dye concentrated into KWB and mycoregenerated the sorbent matrix after 15 days of culture. The mycoregenerated-KWB (MKWB) maintained its REA (79.5 ± 2.0%). Therefore, mycodegradation under SSF was demonstrated as an adequate solution for the final disposal of the adsorbed AB_{161} and the regeneration and reusability of KWB. Further studies on larger-scale and reactor conditions are required to advance into a commercial combined method for treating dye-containing wastewater from the leather industry.

DECLARATIONS

Abbreviations

Acid Blue 161 (AB_{161})

Activated carbon (AC)

Amount of dye uptake at equilibrium (q_e)

Barret, Joyner, and Halenda method (BJH)

Box-Behnken design (BBD)

Brunauer, Emmett, and Teller multipoint method (BET)

Dye removal efficiency by adsorption (REA)

Dye removal efficiency by mycoremediation (REM)

Dye-containing depolymerised-biochar ($KWB\text{-}AB_{161}$)

Fourier Transform Infrared Spectroscopy (FT-IR)

Fungal growth (G)

Growth Area (A)

$KMnO_4$-depolymerised-biochar (KWB)

Laccase (Lac)

Malt Extract Agar (MEA)

Mycoregenerated-KWB (MKWB)

NaOH-depolymerised-biochar (NWB)

Point of zero charges (pH_{pzc})

Response Surface Methodology (RSM)

Scanning Electron Microscopy (SEM)

Solid-state fermentation (SSF)

Specific surface area (S_{BET})

Wood-chip biochar (WB)

X-ray diffraction (XRD)

Acknowledgements

The authors would like to thank the Brazilian Coordination for the Improvement of Higher-Level Personnel (CAPES) for the Research Fellowship "Doctoral Program Abroad (PDSE)" and the Centre for NanoHealth at Swansea University for the technical support.

Authors' contributions

SOM performed the experiments, analysed the data, and drafted the manuscript. JP produced and characterised the biochars and supported data analysis and manuscript edition.

SBL carried out the morphological characterisation of the biochars. MG and PV supervised the overall doctoral project, analysed the data, edited and reviewed the manuscript. DK and SLK supervised the experimental work and edited and reviewed the manuscript. All authors read and approved the final manuscript.

Funding

This work was supported by the European Regional Development Fund/Welsh Government funded BEACON+ research programme (Swansea University) and the Brazilian Coordination for the Improvement of Higher-Level Personnel (CAPES) with the Research Fellowship "Doctoral Program Abroad (PDSE)".

Availability of data and materials

The datasets used and/or analysed during the current study are available from the corresponding author on request.

Ethics approval and consent to participate

Not applicable.

Consent for publication

Not applicable.

Competing interests

The authors declare that they have no known competing interests that could have appeared to influence the work reported in this paper.

REFERENCES

Ahmed, M.J., Okoye, P.U., Hummadi, E.H., Hameed, B.H., 2019. High-performance porous biochar from the pyrolysis of natural and renewable seaweed (*Gelidiella acerosa*) and its application for the adsorption of methylene blue. Bioresour. Technol. 278, 159–164. https://doi.org/10.1016/j.biortech.2019.01.054

Aksu, Z., Tatlı, A.I., Tunç, O., 2008. A comparative adsorption/biosorption study of Acid Blue 161: effect of temperature on equilibrium and kinetic parameters. Chem. Eng. J. 142, 23–39. https://doi.org/10.1016/j.cej.2007.11.005

Arora, D.S., Gill, P., 2001. Comparison of two assay procedures for lignin peroxidase. Enzyme Microb. Technol. 28, 602–605. https://doi.org/10.1016/S0141-0229(01)00302-7

Asgher, M., Noreen, S., Bilal., M., 2017. Enhancing catalytic functionality of *Trametes versicolor* ibl-04 laccase by immobilization on chitosan microspheres. Chem. Eng. Res. Des. 119, 1–11. https://doi.org/10.1016/j.cherd.2016.12.011

Bankole, P.O., Adekunle, A.A., Govindwar, S.P., 2018. Biodegradation of a monochlorotriazine dye, Cibacron Brilliant Red 3b-a in solid state fermentation by wood-rot fungal consortium, *Daldinia concentrica* and *Xylaria polymorpha*: co-biomass decolorization of Cibacron Brilliant Red 3b-a dye. Int. J. Biol. Macromol. 120, 19–27. https://doi.org/10.1016/j.ijbiomac.2018.08.068

Behl, K., Sinha, S., Sharma, M., Singh, R., Joshi, M. et al. 2019. One-time cultivation of *Chlorella pyrenoidosa* in aqueous dye solution supplemented with biochar for microalgal growth, dye decolorization and lipid production. Chem. Eng. J. 364, 552–561. https://doi.org/10.1016/j.cej.2019.01.180

Bernardino, C.A.R., Mahler, C.F., Veloso, M.C.C., Romeiro, G.A., 2017. Preparation of biochar from sugarcane by-product filter mud by slow pyrolysis and its use like adsorbent. Waste Biomass Valor. 8, 2511–2521. https://doi.org/10.1007/s12649-016-9728-5

Bharti, V., Vikrant, K., Goswami, M., Tiwari, H., Sonwani, R.K. et al. 2019. Biodegradation of Methylene Blue dye in a batch and continuous mode using biochar as packing media. Environ. Res. 171, 356–364. https://doi.org/10.1016/j.envres.2019.01.051

Boakye, P., Tran, H.N., Lee, D.S., Woo, S.H., 2019. Effect of water washing pretreatment on property and adsorption capacity of macroalgae-derived biochar. J. Environ. Manage. 233, 165–174. https://doi.org/10.1016/j.jenvman.2018.12.031

Böhmer, U., Frömmel, S., Bley, T., Müller, M., Frankenfeld, K. et al. 2011. Solid-state fermentation of lignocellulotic materials for the production of enzymes by the white-rot gungus *Trametes hirsuta* in a modular bioreactor. Eng. Life Sci. 11, 395–401. https://doi.org/10.1002/elsc.201000162

Braghiroli, F.L., Bouafif, H., Neculita, C.M., Koubaa, A., 2018. Activated biochar as an effective sorbent for organic and inorganic contaminants in water. Water Air Soil Pollut. 229, 1–22. https://doi.org/10.1007/s11270-018-3889-8

Chaukura, N., Murimba, E.C., Gwenzi, W., 2017. Synthesis, characterisation and Methyl Orange adsorption capacity of Ferric Oxide-biochar nano-composites derived from pulp and paper sludge. Appl. Water Sci. 7, 2175–2186. https://doi.org/10.1007/s13201-016-0392-5

Chen, S.H., Ting, A.S.Y., 2015. Biodecolorisation and biodegradation potential of recalcitrant triphenylmethane dyes by *Coriolopsis* sp. Isolated from compost. J. Environ. Manage. 150, 274–280. https://doi.org/10.1016/j.jenvman.2014.09.014

Chen, Y., Lin, Y., Ho, S., Zhou, Y., Ren, N., 2018. Highly efficient adsorption of dyes by biochar derived from pigments-extracted macroalgae pyrolyzed at different temperature. Bioresour. Technol. 259, 104–110. https://doi.org/10.1016/j.biortech.2018.02.094

Copete-Pertuz, L.S., Alandete-Novoa, F., Placido, J., Correa-Londoño, G.A., Mora-Martinez, A.L., 2019. Enhancement of ligninolytic enzymes production and decolourising activity in *Leptosphaerulina* Sp. by co-cultivation with *Trichoderma viride* and *Aspergillus terreus*. Sci. Total Environ. 646, 1536–1545. https://doi.org/10.1016/j.scitotenv.2018.07.387

Copete-Pertuz, L.S., Chanaga, X., Barriuso, J., López-Lucendo, M.F., Martínez, M.J., Camarero, S., 2015. Identification and characterization of laccase-type multicopper oxidases involved in dye-decolorization by the fungus *Leptosphaerulina* sp. BMC Biotechnol. 15, 1–13. http://dx.doi.org/10.1186/s12896-015-0192-2

Daâssi, D., Zouari-Mechichi, H., Frikha, F., Rodríguez-Couto, S., Nasri, M. et al. 2016. Sawdust waste as a low-cost support-substrate for laccases production and adsorbent for azo dyes decolorization. J. Environ. Health Sci. Engineer. 14, 1. https://doi.org/10.1186/s40201-016-0244-0

Dai, Y., Zhang, N., Xing, C., Cui, Q., Sun, Q., 2019. The adsorption, regeneration and engineering applications of biochar for removal organic pollutants: a review. Chemosphere 223, 12–27. https://doi.org/10.1016/j.chemosphere.2019.01.161

Daneshvar, E., Vazirzadeh, A., Niazi, A., Kousha, M., Naushad, M., Bhatnagar, A., 2017. Desorption of Methylene Blue dye from brown macroalga: effects of operating parameters, isotherm study and kinetic modeling. J. Clean. Prod. 152, 443–453. https://doi.org/10.1016/j.jclepro.2017.03.119

Das, R., Bandyopadhyay, R., Pramanik, P., 2018. Carbon quantum dots from natural resource: a review. Mater. Today Chem. 8, 96–109. https://doi.org/10.1016/j.mtchem.2018.03.003

El-Naggar, A., El-Naggar, A.H., Shaheen, S.M., Sarkar, B., Chang, S.X. et al. 2019. Biochar composition-dependent impacts on soil nutrient release, carbon mineralization, and potential environmental risk: A review. J. Environ. Manage. 241, 458–467. https://doi.org/10.1016/j.jenvman.2019.02.044

da Fontoura, J.T., Rolim, G.S., Mella, B., Farenzena, M., Gutterres, M., 2017. Defatted microalgal biomass as biosorbent for the removal of acid Blue 161 dye from tannery effluent. J. Environ. Chem. Eng. 5, 5076–5084. https://doi.org/10.1016/j.jece.2017.09.051

Gomes, C.S., Piccin, J.S., Gutterres, M., 2016. Optimising adsorption parameters in tannery dye-containing effluent treatment with leather shaving waste. Process Saf. Environ. Prot. 99, 98–106. https://doi.org/10.1016/j.psep.2015.10.013

Jaramillo, A.C., Cobas, M., Hormaza, A., Sanroman, M.A., 2017. Degradation of adsorbed azo dye by solid-state fermentation: Improvement of culture conditions, a kinetic study, and rotating drum bioreactor performance. Water Air Soil Pollut. 228:205. https://doi.org/10.1007/s11270-017-3389-2

Jiang, B., Lin, Y., Mbog., J.K., 2018. Biochar derived from swine manure digestate and applied on the removals of heavy metals and antibiotics. Bioresour.Technol. 270, 603–611. https://doi.org/10.1016/j.biortech.2018.08.022

Kalpana, D., Velmurugan, N., Shim, J.H. Oh, B.T., Senthil, K. et al. 2012. Biodecolourisation and biodegradation of reactive Levafix Blue E-RA granulate dye by the white Rot fungus *Irpex lacteus*. J. Environ. Manage. 111, 142–149. https://doi.org/10.1016/j.jenvman.2012.06.041

Katheresan, V., Kansedo, J., Lau, S.J., 2018. Efficiency of various recent wastewater dye removal methods: A review. J. Environ. Chem. Eng. 6, 4676–4697. https://doi.org/10.1016/j.jece.2018.06.060

Kaushik, P., Malik, A., 2009. Fungal dye decolourisation: recent advances and future potential. Environ. Int. 35, 127–141. https://doi.org/10.1016/j.envint.2008.05.010

Li, H.X., Zhang, R.J., Tang, L., Zhang, J.H., Mao, Z.G., 2014. *In vivo* and *in vitro* decolourisation of synthetic dyes by laccase from solid state fermentation with

Trametes sp. SYBC-L4. Bioprocess. Biosyst. Eng. 37, 2597–2605. https://doi.org/10.1007/s00449-014-1237-y

Lian, F., Cui, G., Liu, Z., Duo, L., Zhang, G., Xing, B., 2016. One-step synthesis of a novel n-doped microporous biochar derived from crop straws with high dye adsorption capacity. J. Environ. Manage. 176, 61–68. https://doi.org/10.1016/j.jenvman.2016.03.043

Mann, J., Markham, J.L., Peiris, P., Spooner-Hart, R.N., Holford, P. et al. 2015. Use of olive mill wastewater as a suitable substrate for the production of laccase by *Cerrena* Consors. Int. Biodeter. Biodegr. 99, 138–145. https://doi.org/10.1016/j.ibiod.2015.01.010

Martinez, M.J., Francisco, R.D., Guillen, F., Martinez, A.T., 1996. Purification and catalytic properties of two manganese peroxidase isoenzymes from *Pleurotus Eryngii*. Eur. J. Biochem. 237, 424–432. http://dx.doi.org/10.1111/j.1432-1033.1996.0424k.x

Meili, L., Lins, P.V., Zanta, C.L., Soletti, J.I., Ribeiro, L.M. et al. 2019. MgAl-LDH/biochar composites for Methylene Blue removal by adsorption. Appl. Clay Sci. 168, 11–20. https://doi.org/10.1016/j.clay.2018.10.012

Mella, B., Puchana-Rosero, M.J., Costa, D.E.S., Gutterres, M., 2017. Utilisation of tannery solid waste as an alternative biosorbent for acid dyes in wastewater treatment. J. Mol. Liq. 242, 137–145. https://doi.org/10.1016/j.molliq.2017.06.131

Nautiyal, P., Subramanian., K.A., Dastidar, M.G., 2016. Adsorptive removal of dye using biochar derived from residual algae after *in situ* transesterification: alternate use of waste of biodiesel industry. J. Environ. Manage. 182, 187–197. https://doi.org/10.1016/j.jenvman.2016.07.063

Oliveira, F.R., Patel, A.K., Jaisi, D.P., Adhikari, S., Lu, H., Khanal, S.K., 2017. Environmental application of biochar: Current status and perspectives. Bioresour. Technol. 246, 110–122. https://doi.org/10.1016/j.biortech.2017.08.122

Ortiz-Monsalve, S., Dornelles, J., Poll, E., Ramirez-Castrillon, M., Valente, P., Gutteres, M., 2017. Biodecolourisation and biodegradation of leather dyes by a native isolate of *Trametes villosa*. Process Saf. Environ. Prot. 109, 437–451. https://doi.org/10.1016/j.psep.2017.04.028

Ortiz-Monsalve, S., Valente, P., Poll, E., Jaramillo-Garcia, V., Pegas Henriques, J.A., 2019. Biodecolourization and biodetoxification of dye-containing wastewaters from leather dyeing by the native fungal strain *Trametes villosa* SCS-10. Biochem. Eng. J. 141, 19–28. http://dx.doi.org/10.1016/j.bej.2018.10.002

Ozmen, N., Yesilada, O., 2012. Valorization and biodecolorisation of dye adsorbed on lignocellulosics using white rot fungi. BioResources 7, 1656–1665.

Pandi, A., Kuppuswami, G.M., Ramudu, K.N., Palanivel, S., 2019. A sustainable approach for degradation of leather dyes by a new fungal laccase. J. Clean. Prod. 211, 590–597. https://doi.org/10.1016/j.jclepro.2018.11.048

Park, J.H., Wang, J.J., Meng, Y., Wei, Z., DeLaune, R.D. et al. 2019. Adsorption/desorption behavior of cationic and anionic dyes by biochars prepared at normal and high pyrolysis temperatures. Colloid. Surf. A. 572, 274–282. https://doi.org/10.1016/j.colsurfa.2019.04.029

Placido, J., Capareda, S., 2015. Production of silicon compounds and fulvic acids from cotton wastes biochar using chemical depolymerization. Ind. Crop. Prod. 67, 270–80. https://doi.org/10.1016/j.indcrop.2015.01.027

Placido, J., Bustamante-López, S., Meissner, K.E., Kelly, D.E., Kelly, S.L., 2019a. NanoRefinery of carbonaceous nanomaterials: Complementing dairy manure gasification and their applications in cellular imaging and heavy metal sensing. Sci. Total Environ. 689, 10–20. https://doi.org/10.1016/j.scitotenv.2019.06.390

Placido, J., Bustamante-López, S., Meissner, K.E., Kelly, D.E., Kelly, S.L., 2019b. Comparative study of the characteristics and fluorescent properties of three different biochar derived carbonaceous nanomaterials for bioimaging and heavy metal ions sensing. Fuel Proces. Technol. 196, 106–163. https://doi.org/10.1016/j.fuproc.2019.106163

Placido, J., Bustamante-López, S., Meissner, K.E., Kelly, D.E., Kelly, S.L., 2019c. Microalgae biochar-derived carbon dots and their application in heavy metal sensing in aqueous systems. Sci. Total Environ. 656, 531–539. https://doi.org/10.1016/j.scitotenv.2018.11.393

Puchana-Rosero, M.J., Lima, E.C., Ortiz-Monsalve, S., Mella, B., Costa, D.E.S., Poll, E., Gutterres, M., 2017. Fungal biomass as biosorbent for the removal of Acid Blue 161 dye in aqueous solution. Environ. Sci. Pollut. Res. 24, 4200–4209. https://doi.org/10.1007/s11356-016-8153-4

Rivera-Hoyos, C.M., Morales-Álvarez, E.D., Poutou-Piñales, R.A., Pedroza-Rodríguez, A.M., Rodríguez-Vázquez, R. et al. 2013. Fungal laccases. Fungal Biol. Rev. 27, 67–82. https://doi.org/10.1016/j.fbr.2013.07.001

Rodríguez-Couto, S., Osma, J.F., Toca-Herrera, J.L., 2009. Removal of synthetic dyes by an eco-friendly strategy. Eng. Life Sci. 9, 116–123. https://doi.org/10.1002/elsc.200800088

Salvador, F., Martin-Sanchez, N., Sanchez-Hernandez, R., Sanchez-Montero, M.J., Izquierdo, C., 2015. Regeneration of carbonaceous adsorbents. Part II: Chemical, microbiological and vacuum regeneration. Micropor. Mesopor. Mat. 202, 277–296. https://doi.org/10.1016/j.micromeso.2014.08.019

Saroj, S., Kumar, K., Pareek, N., Prasad, R., Singh, R.P., 2014. Biodegradation of azo dyes Acid Red 183, Direct Blue 15 and Direct Red 75 by the isolate *Penicillium oxalicum* SAR-3. Chemosphere 107, 240–248, 2014. https://doi.org/10.1016/j.chemosphere.2013.12.049

Sewu, D.D., Boakye, P., Jung, H., Woo, S.H., 2017. Highly efficient adsorption of cationic dye by biochar produced with korean cabbage waste. Bioresour. Technol. 224, 206 – 213. https://doi.org/10.1016/j.biortech.2017.08.103

Singh, B., Singh, B.P., Cowie, A.L., 2010. Characterisation and evaluation of biochars for their application as a soil amendment. Soil Research 48, 516–525. https://doi.org/10.1071/SR10058

Song, Z., Lian, F., Yu, Z., Zhu, L., Xing, B., Qiu, W., 2014. Synthesis and characterization of a novel mnox-loaded biochar and its adsorption properties for Cu^{2+} in aqueous solution. Chem. Eng. J. 242, 36–42. http://dx.doi.org/10.1016/j.cej.2013.12.061

Sumalinog, D.A.G., Capareda, S.C., de Luna, M.D.G., 2018. Evaluation of the effectiveness and mechanisms of acetaminophen and Methylene Blue dye adsorption on activated biochar derived from municipal solid wastes. J. Environ. Manage. 210, 255–262. https://doi.org/10.1016/j.jenvman.2018.01.010

Sun, Q.Y., Hong, Y.Z., Xiao, Y.Z., Fang, W., Fang, J., 2009. Decolorisation of textile reactive dyes by the crude laccase produced from solid-state fermentation of agro-by-products. World J. Microb. Biot. 25, 1153–1160. https://doi.org/10.1007/s11274-009-9994-5

Thomas, L., Larroche, C., Pandey, A., 2013. Current developments in solid-state fermentation. Biochem. Eng. J. 81, 146–161. https://doi.org/10.1016/j.bej.2013.10.013

Thommes, M., Katsumi, K., Neimark, A.V, Olivier, J.P., Rodriguez-Reinoso, F. et al. 2015. Physisorption of gases, with special reference to the evaluation of surface area and pore size distribution (IUPAC technical report). Pure Appl. Chem. 87, 1051–1069. https://doi.org/10.1515/pac-2014-1117

Tran, H.N., Lee, CK., Vu, M.T., Chao., H.P., 2017. Removal of copper, lead, Methylene Green 5, and Acid Red 1 by saccharide-derived spherical biochar prepared at low calcination temperatures: Adsorption kinetics, isotherms, and thermodynamics. Water Air Soil Pollut. 228: 401. https://doi.org/10.1007/s11270-017-3582-3

Vikrant, K., Giri, B.S., Raza, N., Roy, K., Kim, K., Rai, B.N., Singh, R.S., 2018. Recent advancements in bioremediation of dye: Current status and challenges. Bioresour. Technol. 253, 355–367. https://doi.org/10.1016/j.biortech.2018.01.029

Vyavahare, D.G., Gurav, R.G., Jadhav, P.P., Patil, R.R., Aware, C.B., Jadhav, J.P., 2018. Response surface methodology optimization for sorption of Malachite Green dye on sugarcane bagasse biochar and evaluating the residual dye for phyto and

cytogenotoxicity. Chemosphere 194, 306–315. https://doi.org/10.1016/j.chemosphere.2017.11.180

Wathukarage, A., Herath, I., Iqbal, M.C.M., Vithanage, M., 2017. Mechanistic understanding of crystal violet dye sorption by woody biochar: implications for wastewater treatment. Environ. Geochem. Health. 41, 1647–1661. https://doi.org/10.1007/s10653-017-0013-8

Wang, H.X., Ng, T.B., 2006. Purification of a laccase from fruiting bodies of the mushroom *Pleurotus eryngii*. Appl. Microbiol. Biotechnol. 69, 521–525. https://doi.org/10.1007/s00253-005-0086-7

Wang, X., Bayan, M.R., Yu, M., Ludlow, D.K., Liang, X., 2017. Atomic layer deposition surface functionalized biochar for adsorption of organic pollutants: improved hydrophilia and adsorption capacity. Int. J. Environ. Sci. Technol. 14, 1825–1843. https://doi.org/10.1007/s13762-017-1300-8

Xu, Y., Liu, Y., Liu, S., Tan, X., Zeng, G. et al. 2016. Enhanced adsorption of Methylene Blue by citric acid modification of biochar derived from water hyacinth (*Eichornia crassipes*). Environ. Sci. Pollut. Res. 23, 23606–23618. https://doi.org/10.1007/s11356-016-7572-6

Zazycki, M.A., Godinho, M., Perondi, D., Foletto, E.L., Collazzo, G.C., Dotto, G.L., 2018. New biochar from pecan nutshells as an alternative adsorbent for removing Reactive Red 141 from aqueous solutions. J. Clean. Prod. 171, 57–65. https://doi.org/10.1016/j.jclepro.2017.10.007

Zeng, G., Cheng, M., Huang, D., Lai, C., Xu, P., Wei, Z., Li, N., Zhang, C., He, X., He, Y., 2015. Study of the degradation of methylene blue by semi-solid-state fermentation of agricultural residues with *Phanerochaete chrysos*porium and reutilization of fermented residues. J. Waste Manag. 38, 424–430. https://doi.org/10.1016/j.wasman.2015.01.012

Zhu, K., Wang, X., Chen, D., Ren, W., Lin, H., 2019. Wood-based biochar as an excellent activator of peroxydisulfate for Acid Orange 7 decolorization. Chemosphere 231, 32–40. https://doi.org/10.1016/j.chemosphere.2019.05.087

LIST OF TABLES AND FIGURES

Table 1

Experimental ranges and levels of the Box-Behnken design

Variable (Units)	Range and level		
	–1	0	1
pH, X_1	3	5	7
Initial dye concentration, X_2 (mg L^{-1})	100	200	300
Sorbent dosage, X_3 (g L^{-1})	1	2	3

Table 2

Box-Behnken experimental design matrix and responses

Run	Variable			Response (REA, %)	
	X_1	X_2	X_3	Experimental	Predicted
1	0	–1	1	85.7	85.5
2	0	0	0	80.6	80.7
3	–1	1	0	46.8	46.2
4	1	0	1	73.8	73.4
5	0	1	–1	42.1	42.2
6	0	0	0	80.4	80.7
7	1	0	–1	65.5	65.4
8	0	1	1	47.5	48.0
9	–1	0	1	77.4	78.4
10	–1	–1	0	92.4	92.5
11	–1	0	–1	76.2	77.6
12	1	1	0	45.1	45.0
13	1	–1	0	76.0	76.5
14	0	0	0	80.5	80.7
15	0	–1	–1	83.0	82.5
16	0	0	0	81.1	80.7
17	0	0	0	80.9	80.7

Table 3

Nutrient conditions of the solid-state fermentation with *T. villosa* SCS-10

Nutrient supply condition	Nutrient		
	Malt extract (%)	Glucose (%)	Peptone (%)
High, T_1	1	1	0.5
Reduced, T_2	1	0	0.5
Low, T_3	0	1	0.5
Non-addition, T_4	0	0	0

Table 4

Physicochemical properties of WB and KWB and comparison with those from literature

Adsorbent	S_{BET}[a] ($m^2\ g^{-1}$)	Pore diameter (nm)	Pore volume ($cm^3\ g^{-1}$)	pH_{pzc}[b]	q_e (mg g^{-1})[c]	Dye	Reference
WB[d]	3.4	0.61	0.008	4.5	23.6 ± 0.4	AB_{161}	This work
NWB[e]	22.6	0.59	0.040		30.5 ± 0.8	AB_{161}	This work
KWB[f]	50.4	1.90	0.081		46.7 ± 0.4	AB_{161}	This work
Cattle hair biomass waste	0.9	2.91	0.0007	6.5	104.8	AB_{161}	Mella et al. (2017)
Microalgae biomass	3.5	6.63	0.008	4.2	75.8	AB_{161}	da Fontoura et al. (2017)
T. villosa biomass	1.3	3.76	0.001	2.2	221.6	AB_{161}	Puchana-Rosero et al. (2017)
Fe_2O_3 impregnated pulp and paper sludge biochar	174	1.70–300	3.5	2.1	22.0	Methyl orange	Chaukura et al. (2017)
5Al coated Black willow wood biochar	27.9	–	0.024	–	35.0	Methylene blue	Wang et al. (2017)
Wood-chip biochar	<0.01	2597	–	–	110.0	Congo Red	Sewu et al. (2017)
				–	195.6	Cristal violet	
Pecan nutshell biochar	93	1.20	0.0055	–	130	Reactive Red 141	Zazycki et al. (2018)
Algae biochar	167.0	–	–	–	51.3	Congo Red	Nautiyal et al. (2016)

[a] BET surface area; [b] pH value corresponding to the point of zero charges; [c] Amount of dye uptake at equilibrium; [d] Wood-chip biochar (WB); [e] NaOH-depolymerised biochar (NWB); [d] $KMnO_4$-depolymerised biochar (KWB).

Table 5

Desorption of AB_{161} from KWB using different eluents

Compound	Chemical formula	Concentration (M)	Dye desorption (%)
Ethanol	C_2H_5OH	1	50.2 ± 4.76
Methanol	CH_3OH	1	38.6 ± 4.05
Sodium hydroxide	NaOH	1	21.2 ± 2.54
Sodium chloride	NaCl	1	18.8 ± 0.92
Acetic Acid	CH_3COOH	1	4.2 ± 0.99
Hydrogen chloride	HCl	1	2.6 ± 0.25
Distilled water	H_2O	–	2.0 ± 0.39

Table 6

Solid-state fermentation with *Trametes* strains and dye removal

Strain	Support	Laccase activity	Dye name (Dye removal, %)	Biodegradation Process	Reference
T. villosa	WB and KWB	750 U L^{-1}	Acid Blue 161 (91)	*In vivo*	This work
T. versicolor	Corncobs waste	911 U mL^{-1}	Reactive Blue 21 (89)	*In vitro*	Asgher et al. (2017)
T. versicolor	Corncob waste	8.4 U g^{-1}	Red 40 (96)	*In vivo*	Jaramillo et al. (2017)
Trametes sp.	Cassava residue	150 U L^{-1}	Indigo Carmine (90–99)	*In vivo* and *in vitro*	Li et al. (2014)
T. trogii and *T. versicolor*	Wheat bran		Astrazon Blue (69–86)	*In vivo*	Ozmen and Yesilada (2012)
T. versicolor	Rape stem, wheat bran, peanut shell and rice hull	2 *x* 10^6 U g^{-1}	Levafix Blue (100)	*In vitro*	Sun et al. (2009)
T. hirsuta	Pine wood chips and orange peels	484 U L^{-1}	ns.[a]	ns.	Böhmer et al. (2011)
T. pubescens	Sunflower seed shells	5603 U L^{-1}	R Brilliant Blue R (50–94)	*In vivo*	Rodríguez-Couto et al. (2009)

[a] Not studied

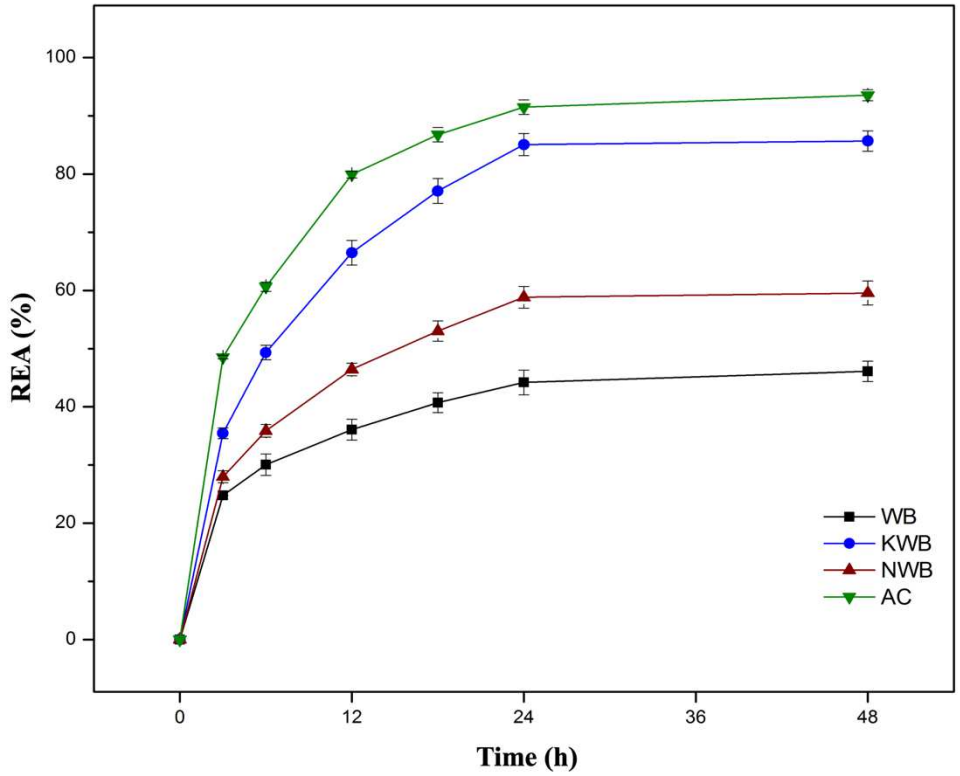

Figure 1**.** Profile of dye removal efficiency by adsorption (REA) into different wood-chip biochar derived materials and activated carbon.

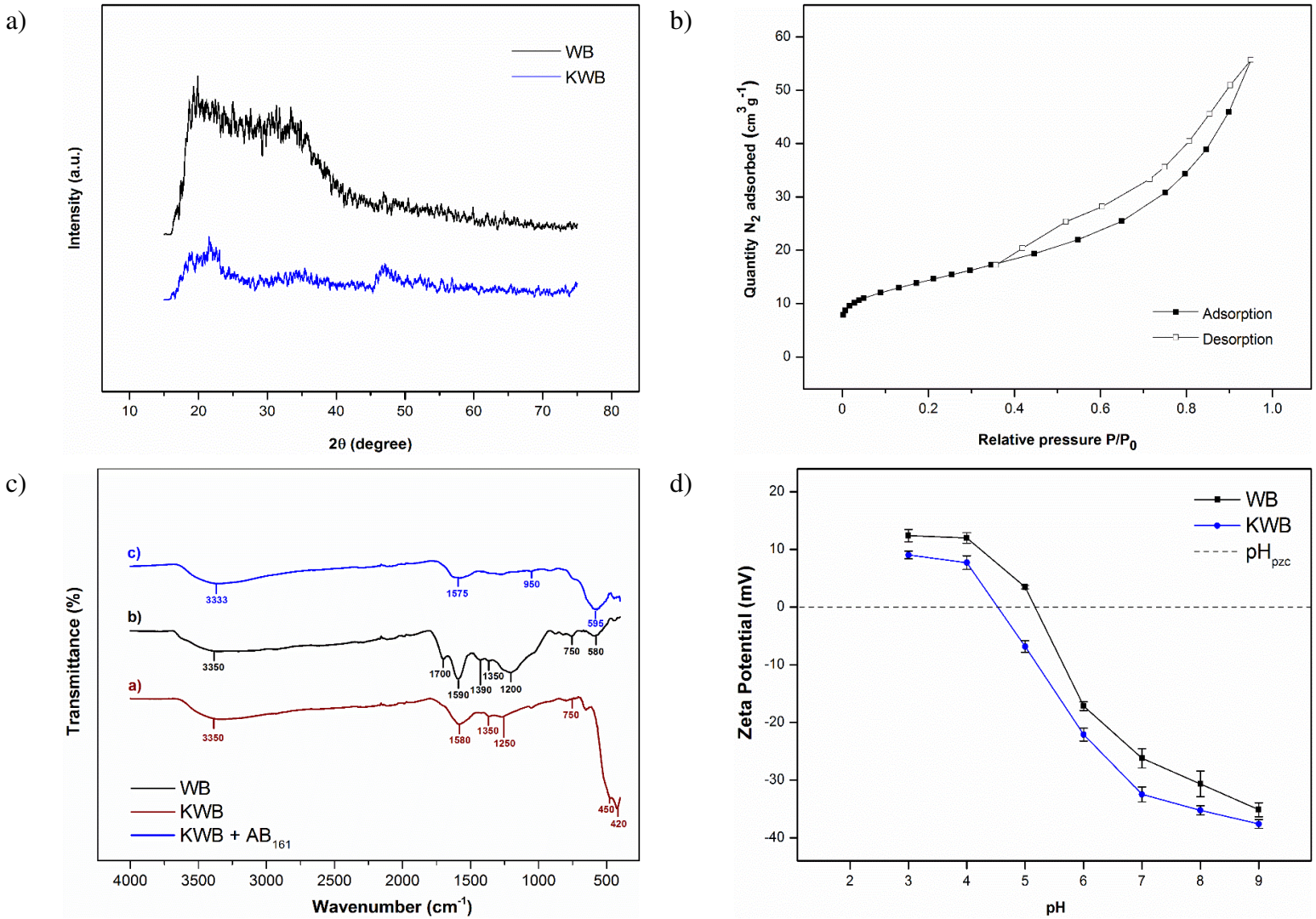

Figure 2. Characterisation of WB and KWB: *a)* XRD spectrum; *b)* N_2 adsorption/desorption isotherm; *c)* FT-IR spectrum; *d)* Zeta potential

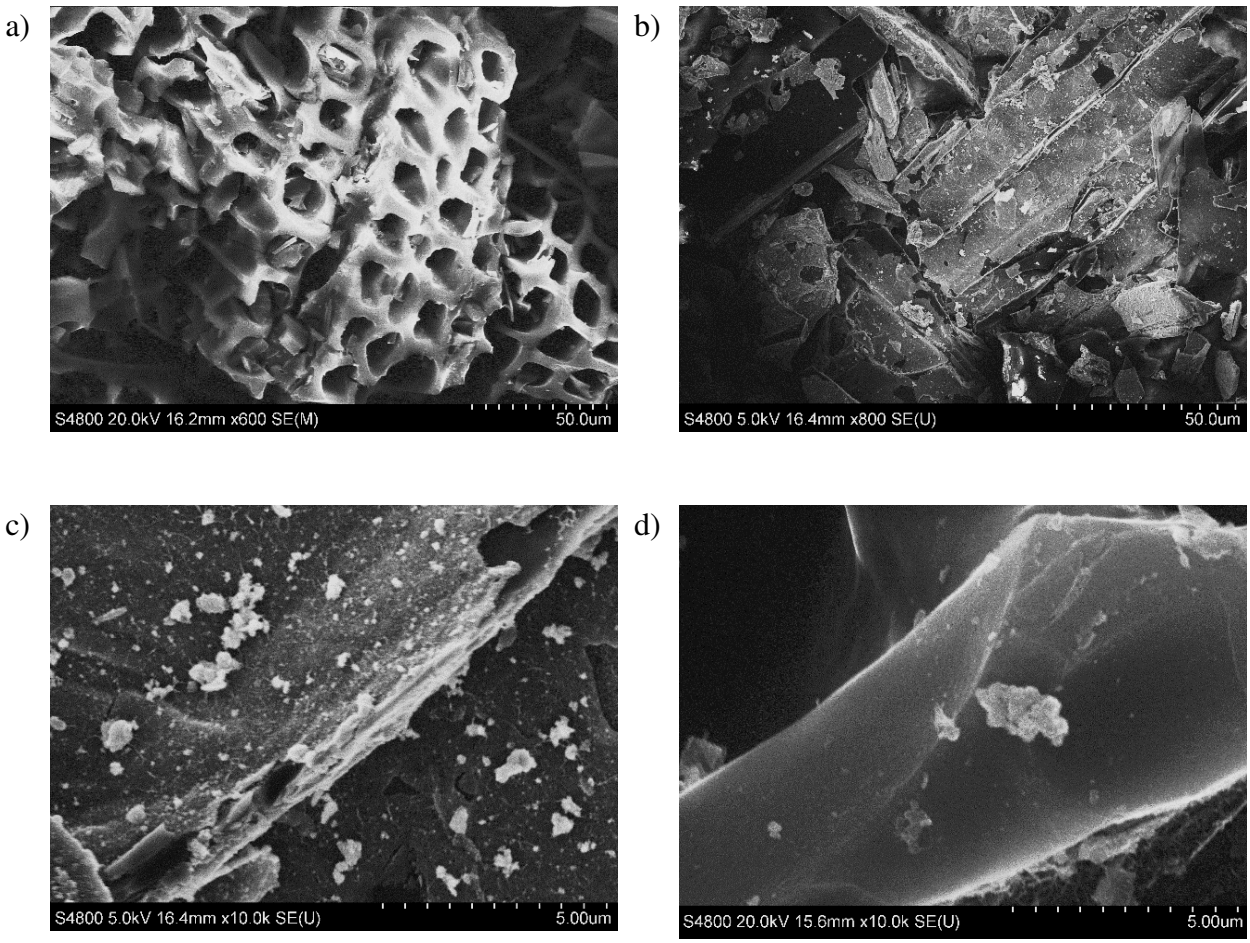

Figure 3. SEM micrographs: *a)* Wood-chip biochar (WB); *b)* $KMnO_4$-depolymerised biochar (KWB); *c)* KWB before AB_{161} adsorption (10 K X); *d)* KWB after AB_{161} adsorption (KWB-AB_{161}) (10 K X)

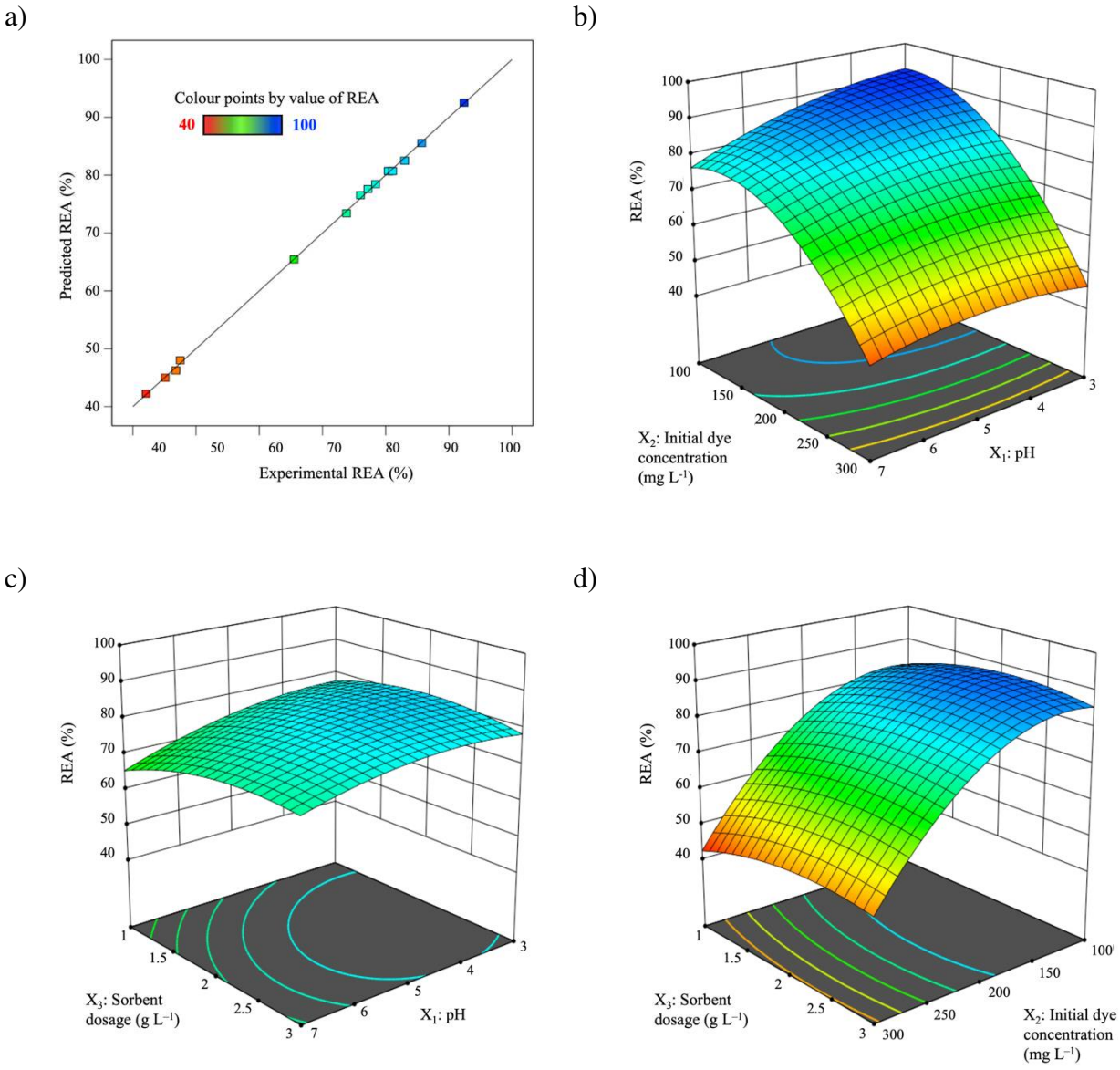

Figure 4. *a)* Plot of the experimental and predicted dye removal efficiency by adsorption (REA);

Response surface 3D plots showing the effect of *b)* pH and initial dye concentration (at sorbent dosage 2 g L^{-1}), *c)* pH and sorbent dosage (at initial dye concentration 200 mg L^{-1}) and *d)* sorbent dosage and initial dye concentration (at pH 5.0) on the dye removal efficiency.

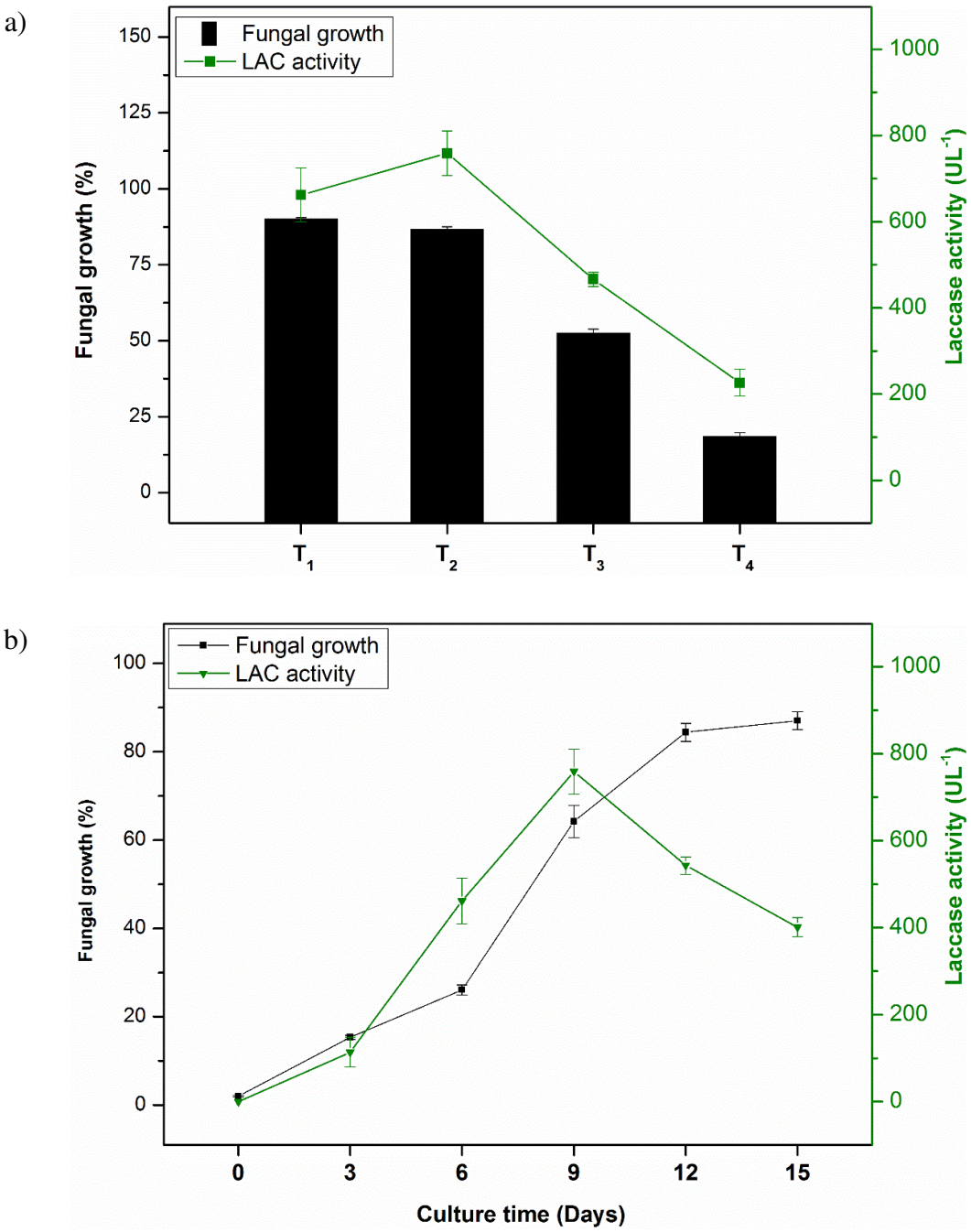

Figure 5. Fungal growth and laccase activity during SSF with *T. villosa* SCS-10: *a)* Effect different nutrient conditions: high nutrient supply (T_1), reduced nutrient supply (T_2), low nutrient supply (T_3) and non-addition (T_4), on the fungal growth (column) and laccase activity (solid line); *b)* Profile of fungal growth and laccase activity during the SSF with the reduced nutrient supply (T_2).

a)

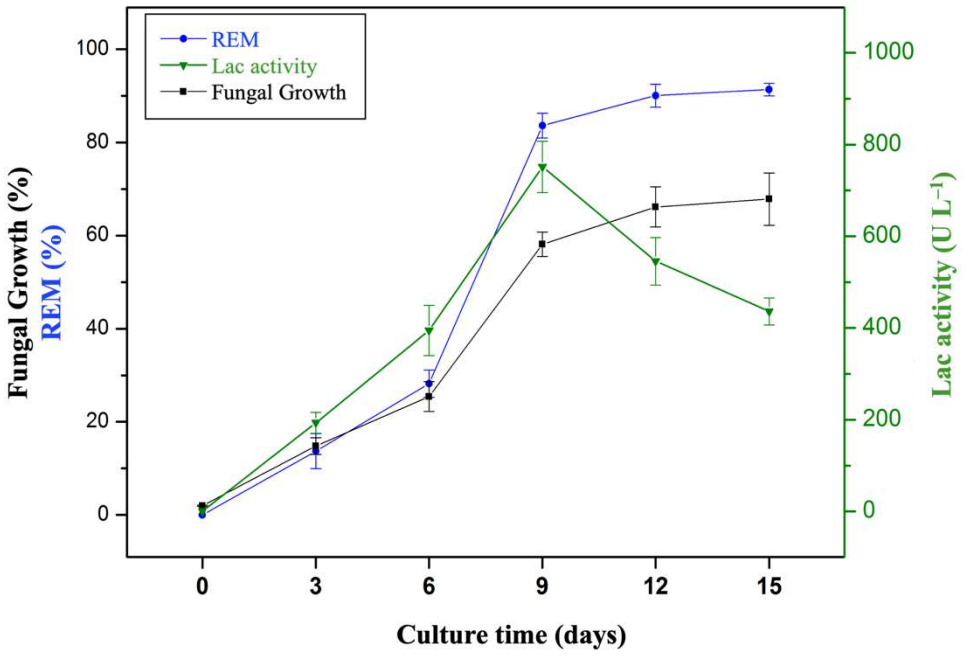

b)

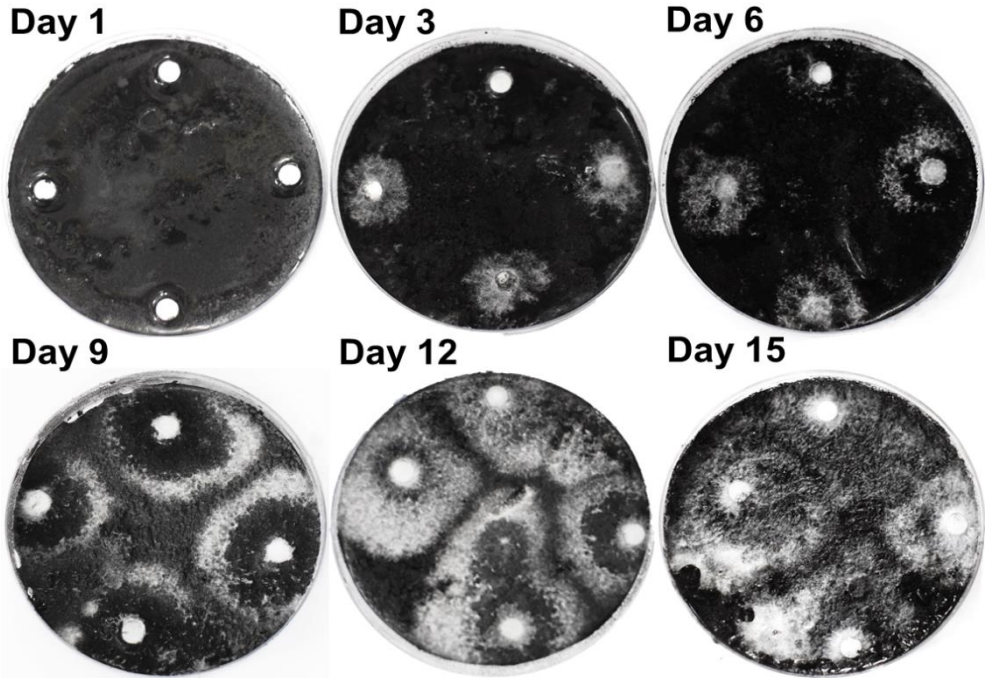

Figure 6. Dye removal of adsorbed AB_{161} by solid-state fermentation with *T. villosa*: *a)* Profile of fungal growth, laccase activity and dye removal by mycoremediation (REM); *b)* Photographs of *T. villosa* SCS-10 growth.

a)

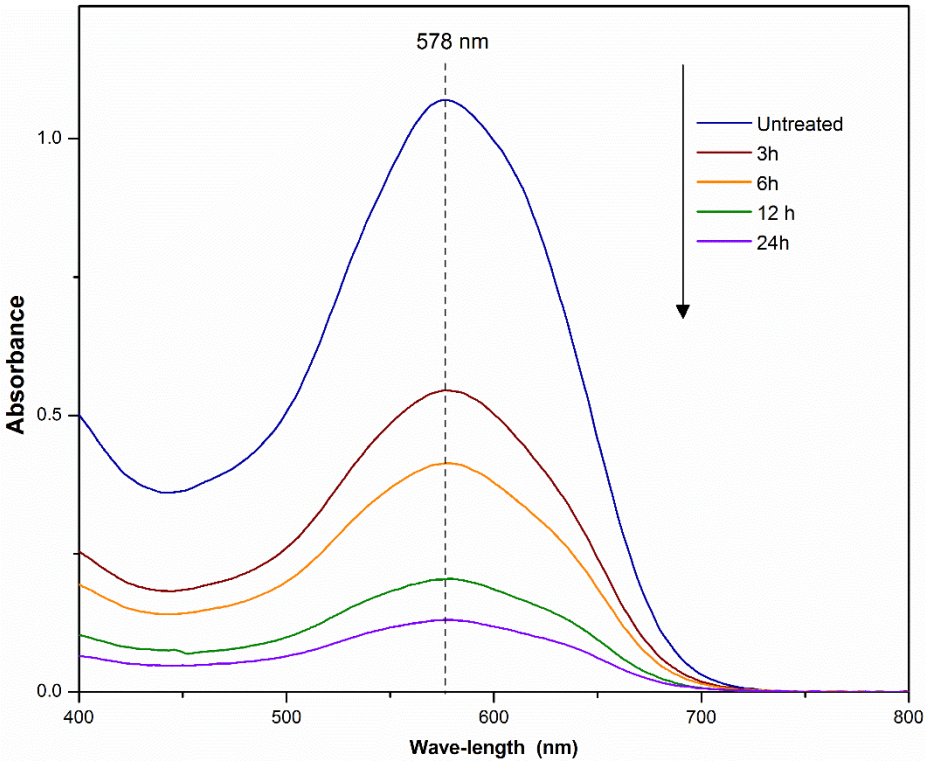

b)

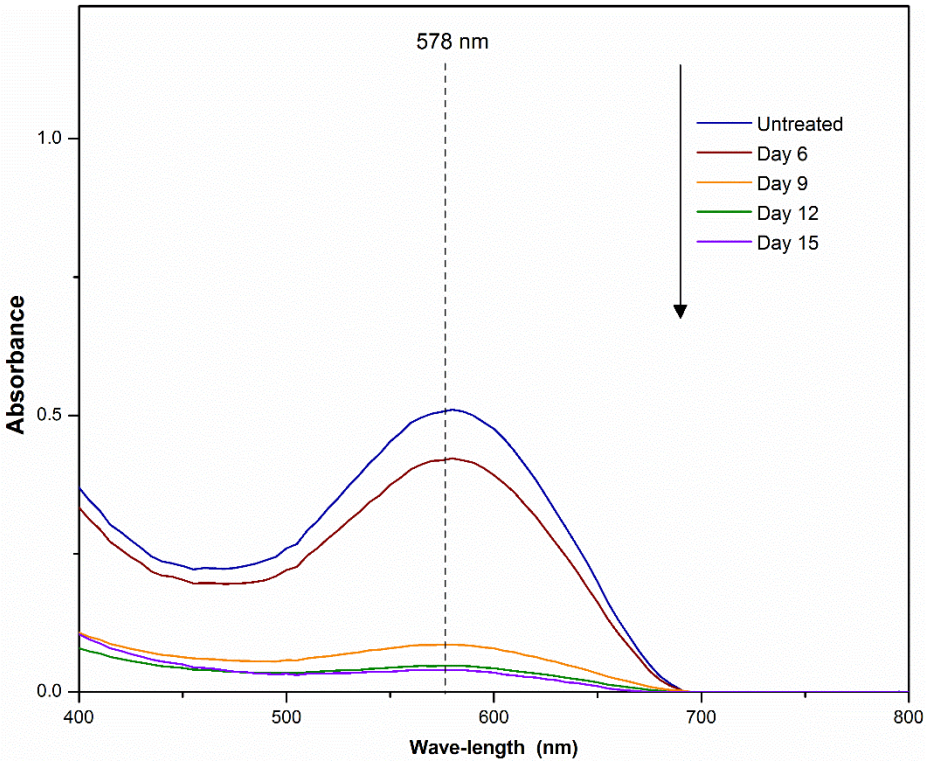

Figure 7. UV-vis spectrum analysis during *a)* AB_{161} adsorption into KWB; *b)* AB_{161} biodegradation by solid-state fermentation by *Trametes villosa* SCS-10.

Figures

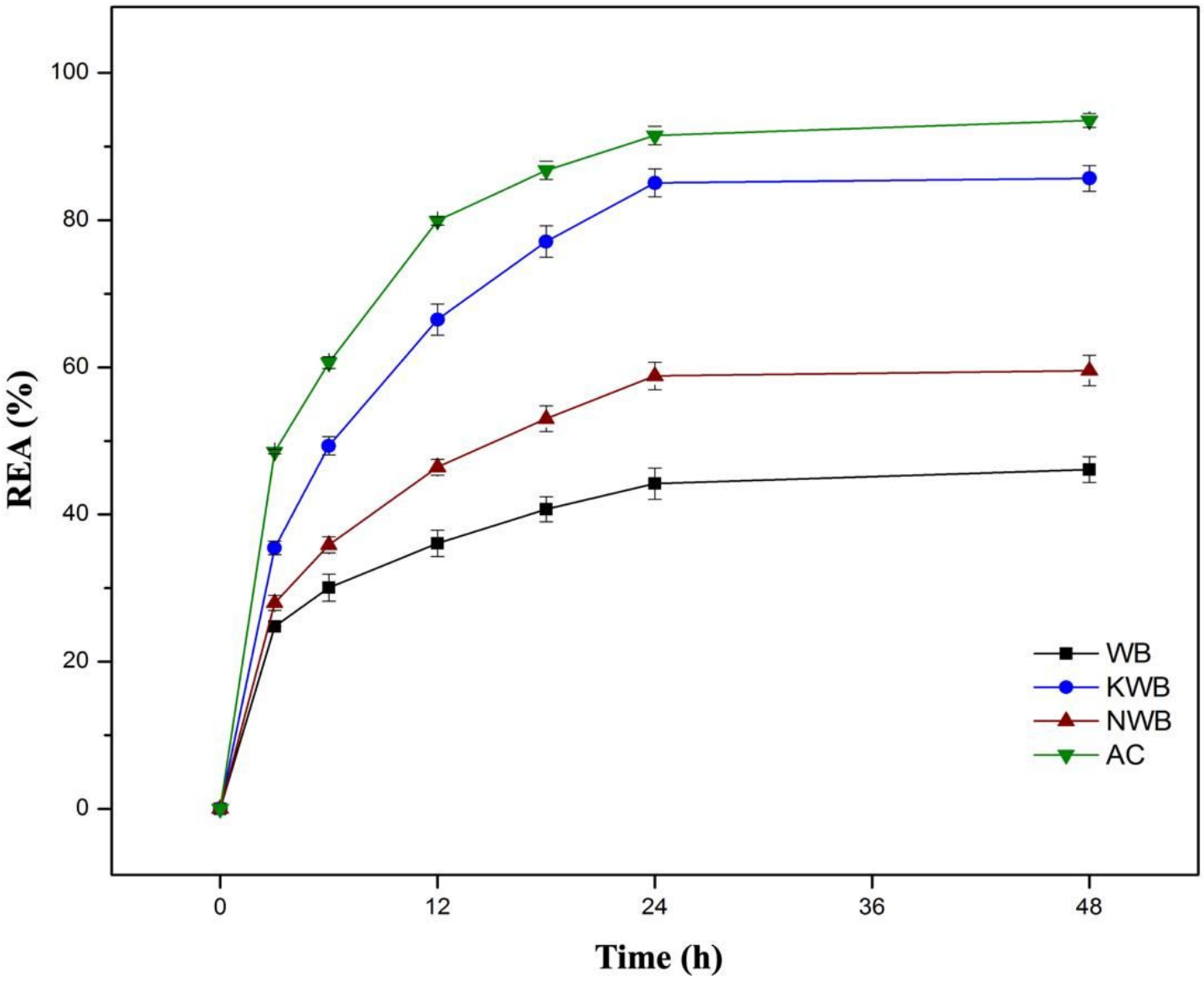

Figure 1

Profile of dye removal efficiency by adsorption into different wood-chip biochar derived materials.

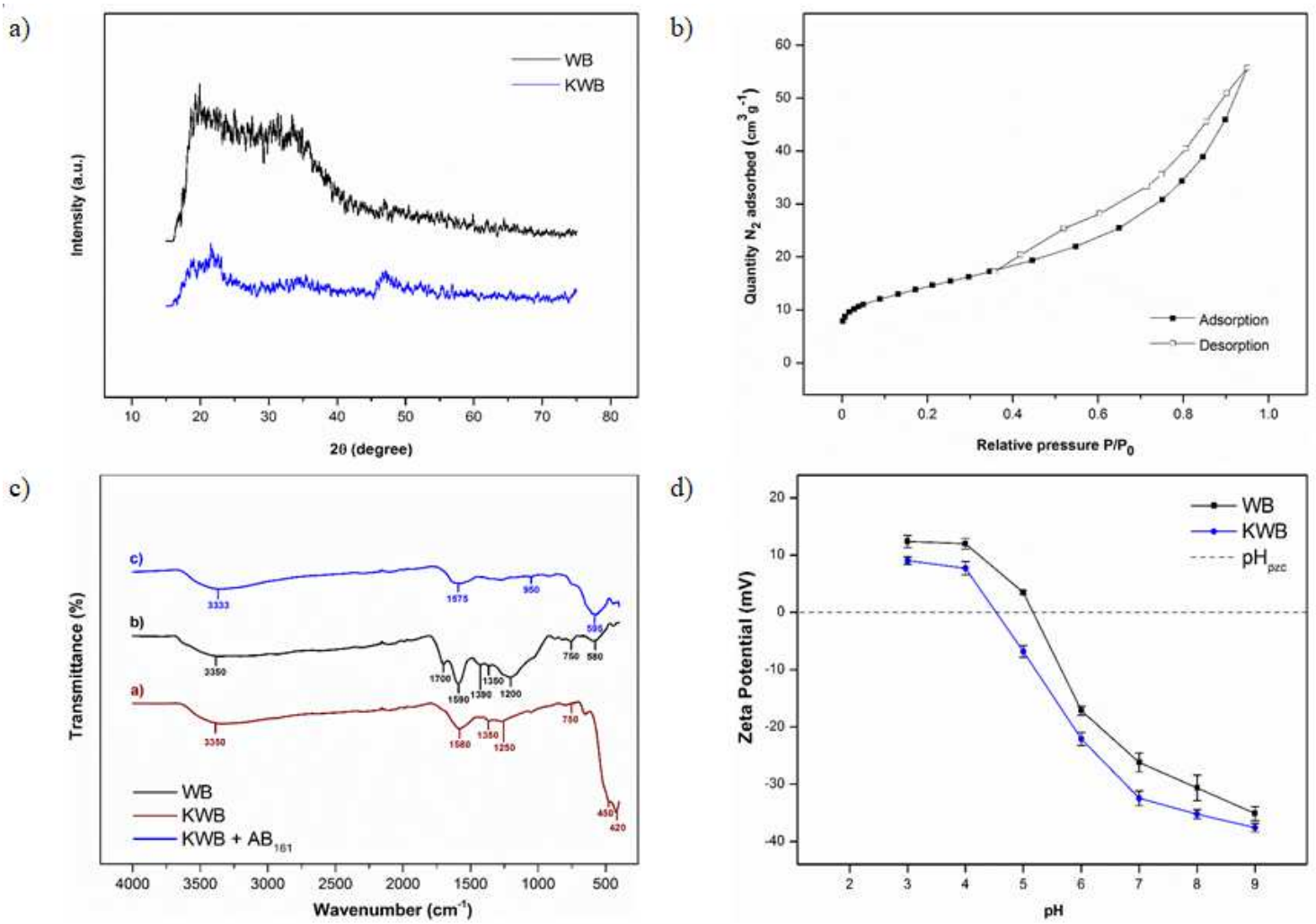

Figure 2

Characterisation of WB and KWB.

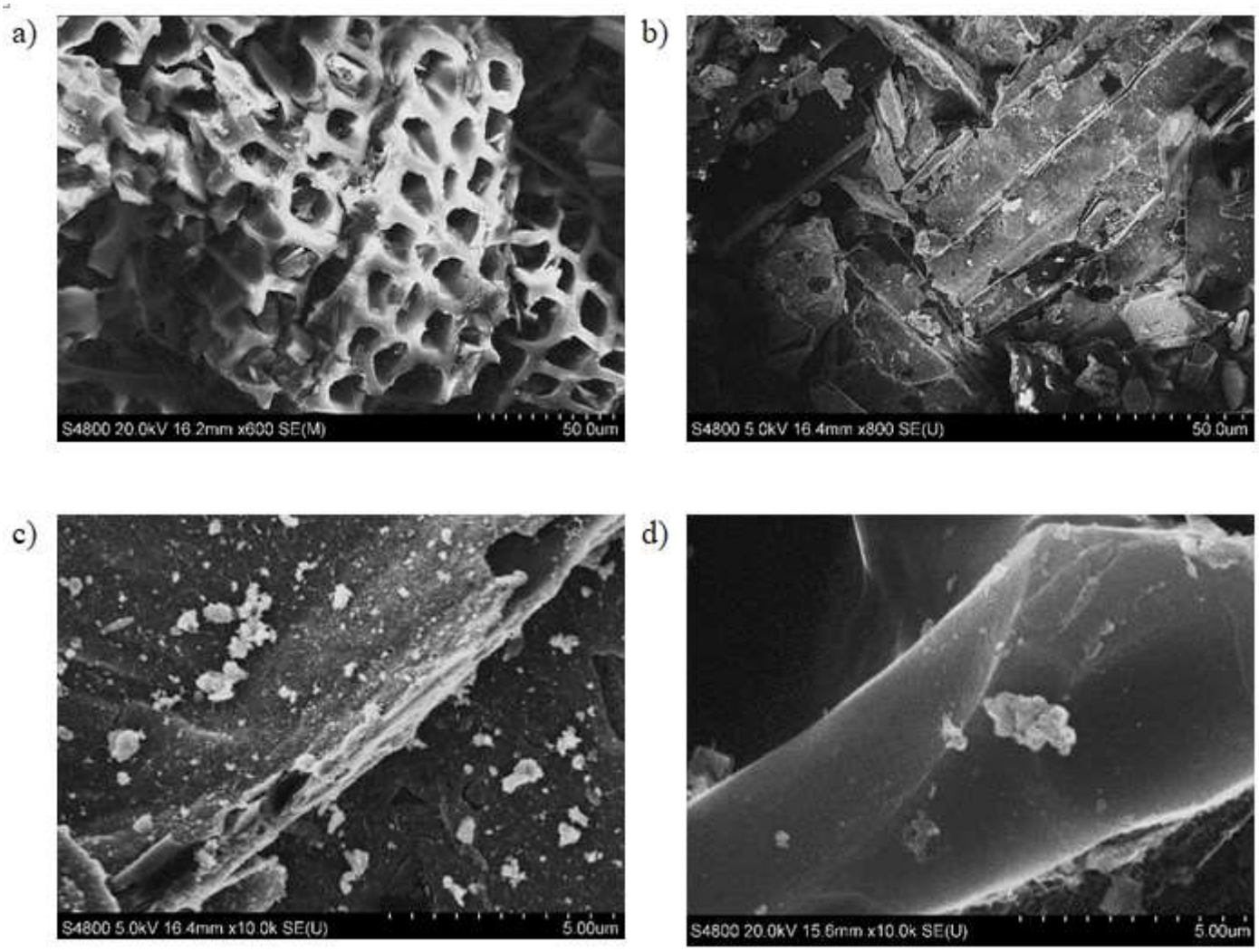

Figure 3

SEM micrographs of WB and KWB.

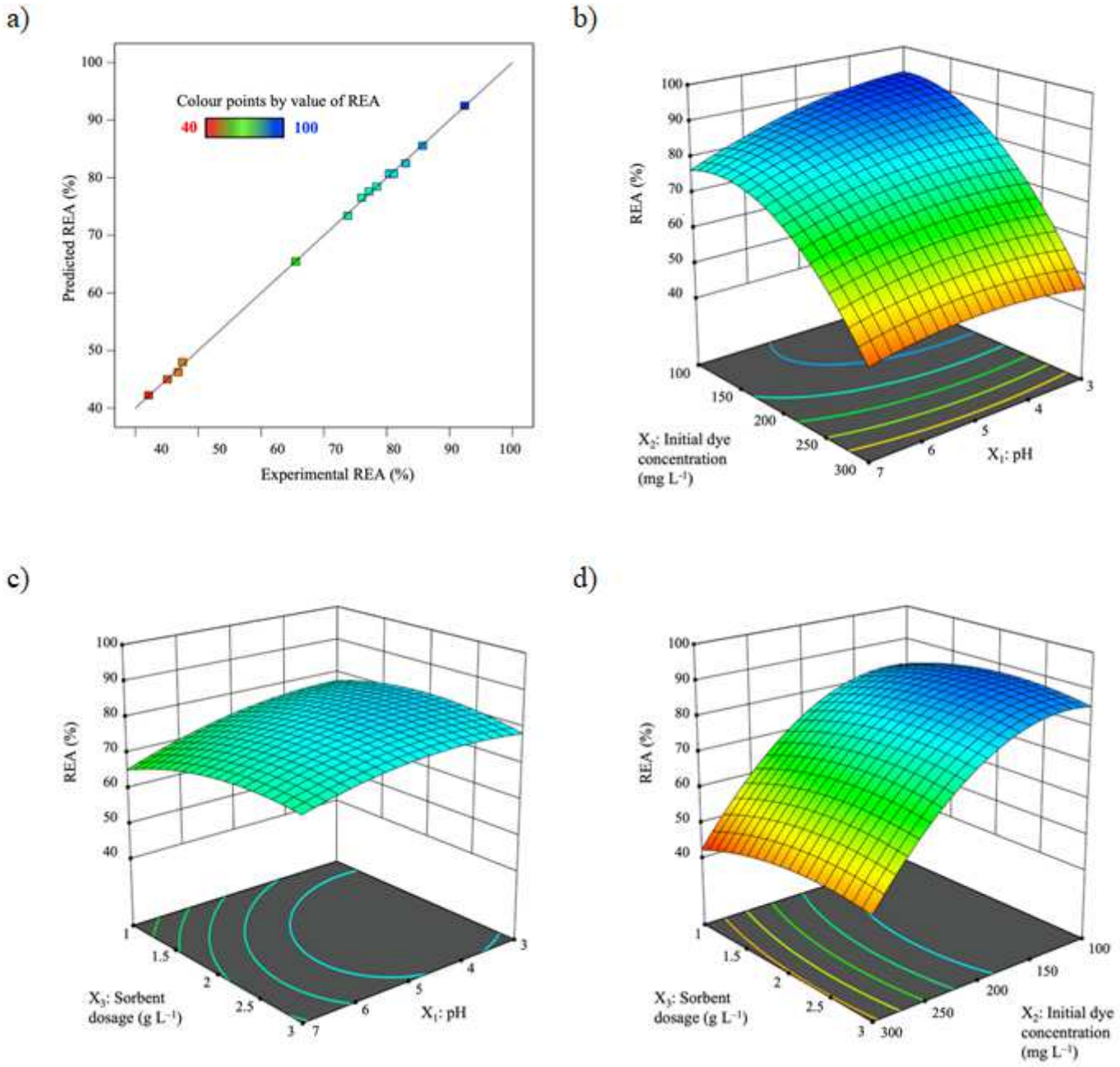

Figure 4

Response surface plots showing the effect of the combined operational variables on the dye removal efficiency.

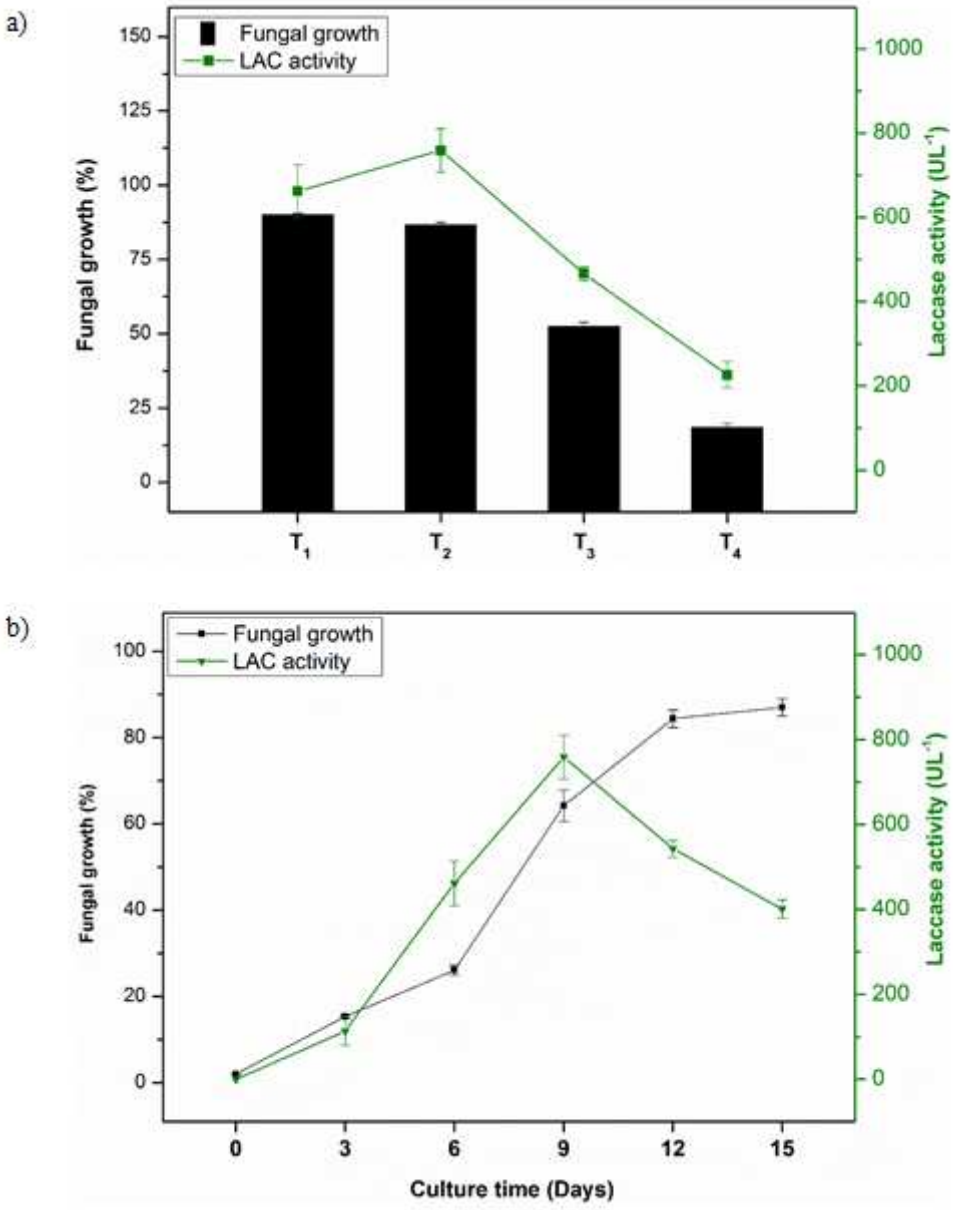

Figure 5

Fungal growth and laccase activity of T. villosa SCS-10 during the solid-state fermentation.

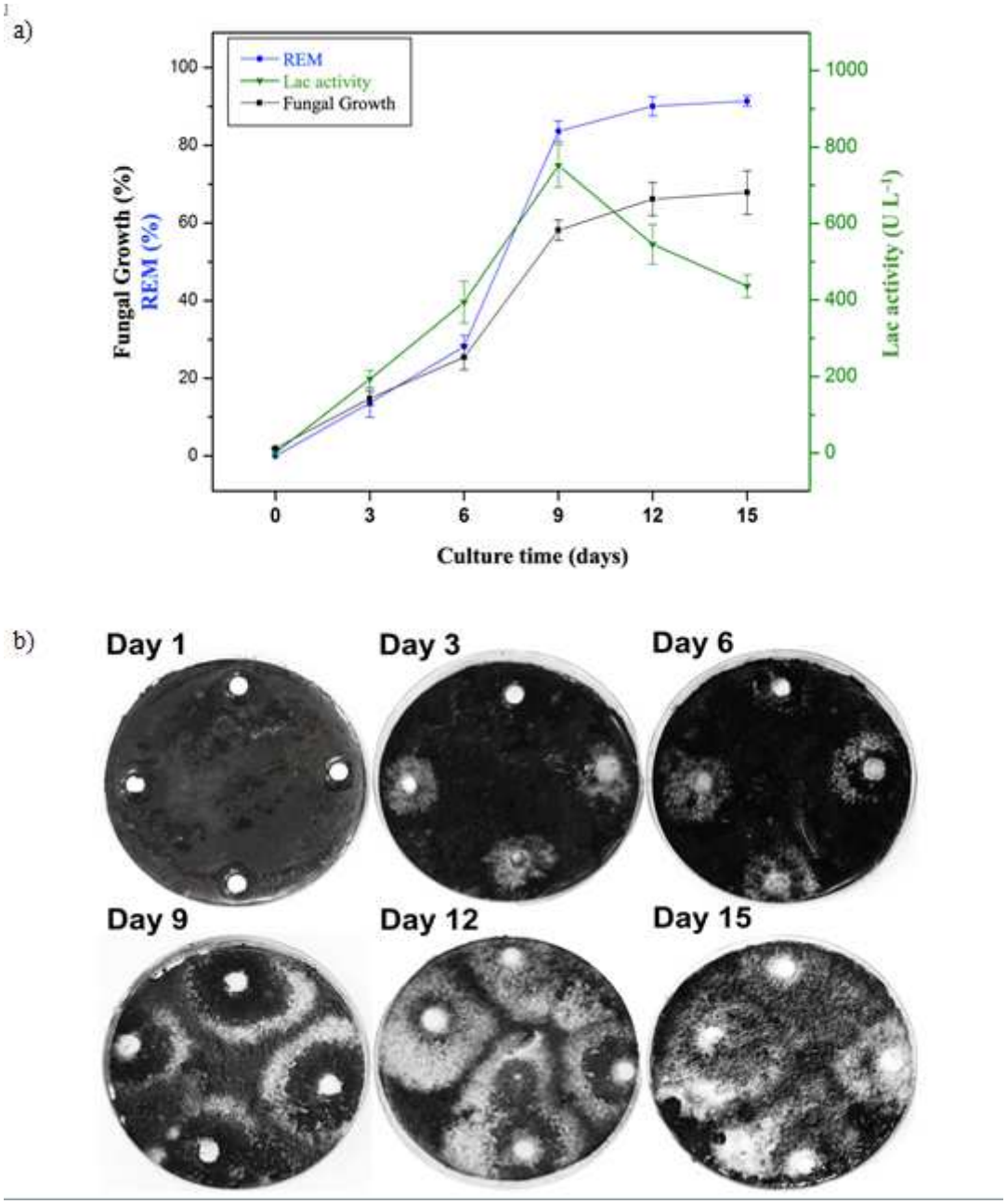

Figure 6

Dye removal of the adsorbed AB161 by solid-state fermentation with T. villosa SCS-10.

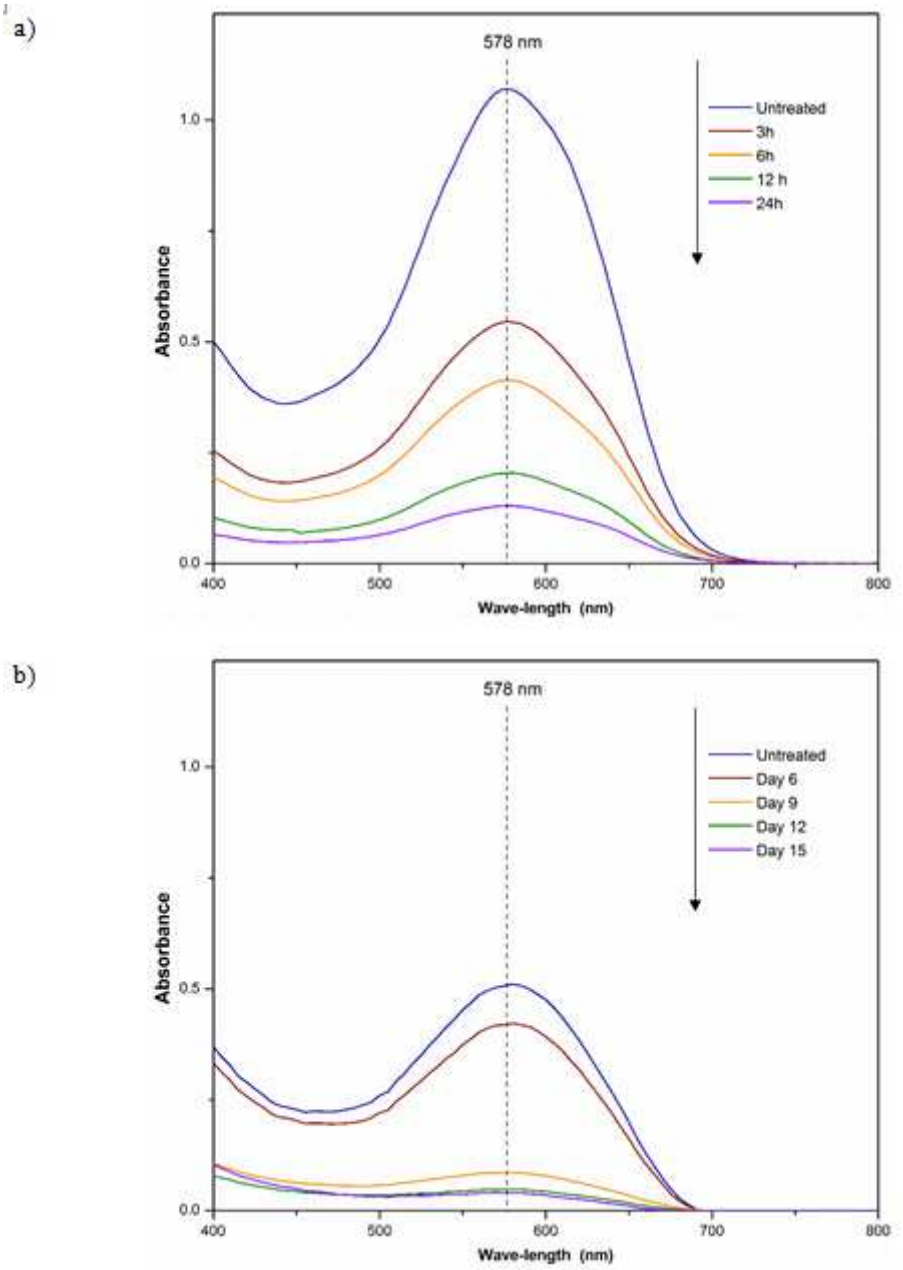

Figure 7

UV–vis spectrum analysis.

Supplementary Files

This is a list of supplementary files associated with this preprint. Click to download.

- GraphicalAbstractOrtizMonsalveBB2020.Tiff
- SupplementarymaterialOrtizMonsalveBB2020.docx